UNIVERSITY OF OKLAHOMA

GRADUATE COLLEGE

MULTI-TEMPORAL LAND SURFACE TEMPERATURE AND VEGETATION GREENNESS IN URBAN GREEN SPACES OF PUEBLA, MEXICO

A THESIS

SUBMITTED TO THE GRADUATE FACULTY

in partial fulfillment of the requirements for the

Degree of

MASTER OF SCIENCE

By

FILOTEO GOMEZ-MARTINEZ
Norman, Oklahoma
2020

MULTI-TEMPORAL LAND SURFACE TEMPERATURE AND VEGETATION GREENNESS IN URBAN GREENS PACES OF PUEBLA, MEXICO.

A THESIS APPROVED FOR THE

DEPARTMENT OF GEOGRAPHY AND ENVIRONMENTAL SUSTAINABILITY

BY THE COMMITTEE CONSISTING OF

Dr. Kirsten de Beurs, Chair

Dr. Jennifer Koch

Dr. Jeffrey Widener

I dedicate my thesis to my parents: Eusebio Gomez Morales and Justina Martinez Vasquez. My father only went to school up through second grade, and my mother never had the opportunity to go to school at all. Despite their lack of educational experience, they always supported the pursuit of my educational goal of *wejën kajen may'aj Naaxwiin Ja'ay* (learning something useful for our home planet and for the 'little' people living on it, although 'little' yet very destructive and fragile at the same time). To them I say, "*Dios kujuuyëbë, mijts* (Thank you, you are the reason for my existence)."

Acknowledgments

I am grateful for the privilege of working with Dr. Kirsten de Beurs. She is the reason I am finishing this academic journey. From when I started the program to the times when I felt like running away from school, and up until the completion of this work, she continuously provided wise guidance, extreme patience, and an extraordinary level of human kindness. Thank you!

To my committee members, Dr. Jennifer Koch and Dr. Jeff Widener, I appreciate your time and energy on reading and providing feedback. Thank you for also participating in this process!

Ever since 2014, when I joined the department as an undergrad transfer student from a community college, I have learned so much from the DGES professors, particularly Dr. Robert Rundstrom, Dr. Randy Peppler, Dr. Scott Greene, Dr. Mary Lawhon, Dr. Mike Wimberly, Dr. Tom Neeson and Dr. Bruce Hoagland. To my fellow graduate student colleagues, especially to, Dolly, Victoria, James, Ethan, Jorge and Jose. Thank you all!

Finally, I am grateful for Laurel's support and counsel and for Rafael's constant cheers with "Tu puedes!"

Table of Contents

List of Tables

List of Figures

Abstract

Urban heat islands (UHI) are a global problem that is likely to increase in the future as our global urban population increases. Multiple studies conclude that urban green spaces and urban waterbodies can reduce UHI impacts, as green spaces provide many environmental and social benefits for the well-being of the residents. However, previous studies often treat urban green spaces (UGS) as static, and other studies greatly limit the number of UGS investigated. Cognizant to these shortcomings, I investigate eighty UGS in Puebla, Mexico, over a 33-year period (1986-2019), with the goal of improving our understanding of UGS characteristics that provide the most cooling to remediate UHI impact. I personally visited 73 of the UGS and recorded the land cover types as well as other characteristics to provide a good baseline understanding of most of the UGS in the study. I also used visible, infrared, and thermal data recorded by the Landsat 5, 7 and 8 sensors. First, I calculated the normalized difference vegetation index (NDVI) for each satellite image. Next, I standardized these NDVI values to mitigate seasonal differences and calculated the slope, p-values, and adjusted r-squared for the relation against time. To retrieve the land surface temperature (LST) from the thermal bands between 2000 and 2019, I applied the Radiative Transfer Equation (RTE). I found that UGS with Indian Laurel vegetation cover were much greener and remained relatively stable compared to UGS with mixed vegetation cover. Similarly, UGS with large waterbodies were cooler than UGS with small water cover. My results show that larger UGS were significantly cooler ($p<0.01$) and that the size of the UGS can explain almost 30% of the LST variability. Furthermore, greener UGS were significantly cooler ($p<0.01$), although this relationship appeared to strengthen over time, with only 16.5% of the variability in LST explained by NDVI in 2000, which increased to 42% by 2019.

Chapter 1: Introduction

"…[humanity] must rise above the earth… and beyond… to fully understand the world in which [we] live." (*Socrates, 500 B.C.E.*)

Remote sensing (RS) allows researchers to study objects or phenomena (land cover, water, or the cryosphere) from a distance (Tucker, C. J. 1979). RS is a science because it obtains relative and absolute measurements, interprets the results, and draws meaningful conclusions; it is a tool because the collected information can be used to draw conclusions that can be used to make inventories of resources and solve ecological problems (Moore, G. K. 1979). There are two types of RS, passive and active, and their measurements utilize electromagnetic energy measurements. Passive RS or passive sensors can only record if the sun is illuminating the earth. The solar energy is either reflected (in the visible and near-infrared wavelengths) or absorbed and then re-emitted (in the thermal infrared wavelengths). Active RS or active sensors do not depend on solar illumination to acquire information from an object. One of them is Radio Detection and Ranging (RADAR); its wavelengths are long enough to penetrate clouds. RADAR uses low frequencies (long wavelengths), in the microwave region ranging from millimeters, meter, and beyond. The other active remote sensing type is Light Detection and Ranging (LiDAR), which uses a laser or pulsed lights. These pulses bounce off from the object and return to the sensor. LiDAR uses both optical and infrared wavelengths.

In 1972, NASA launched its first Earth Resource Technology Satellite (ERTS-1) series, or Landsat 1(William & Carter, 1976). Since then, Landsat 2, Landsat 3, Landsat 4, Landsat 5, Landsat 6, Landsat 7. The most recent and still active Landsat 8 (L8), launched on February 11, 2013 (USGS, 2020). Landsat-9 and its associated instruments is expected to be launched mid-

2021 (USGS Landsat 9, 2020). This study uses Landsat 5 TM (L5), Landsat 7 ETM+ (L7), and Landsat 8 OLI and TIRS (L8), all are passive remote sensing sensors, sun-synchronous orbit with a 16-day repeat cycle. L5 was launched in March 1, 1984, with altitude of 705 km (438 mi) and transmitted over 2.5 million images of land surface around the world, inclined at 98.2 degrees and circle earth every 99 minutes. L7, launched on April 15, 1999 and has similar specifications as L5. L8 has two sensors: The Operational Land Imager and the Thermal Infra-Red Sensors. L8, orbits earth in a sun-synchronous, near-polar altitude of 705 km (438 mi) (USGS, 2020). NASA and the European Space Agency (ESA) both provide open-access global remotely sensed data. These organizations have the mission to advance scientific knowledge to understand planet earth as a system, preserve the environment, and address global environmental issues to benefit the global community (NASA's vision and Mission statement, and ESA's About, 2020).

Remote Sensing data are distinguished by four types of resolution characteristics: 1) Spatial resolution refers to the instantaneous field of view, or the size of one grid cell (pixel) and is usually measured in meters. The spatial resolution of the optical bands for Landsat are 30m. The spatial resolution of the thermal bands is 60m for Landsat 5, and 100m for Landsat 8; 2) The temporal resolution defines how often a land surface is sensed, the Landsat sensors typically have a 16-day repeat cycle, with an 8-day offset between L5 and L8, allowing for images approximately every 8 days from one of the sensors; 3) Radiometric resolution is the ability of the sensor to differentiate tonal variation measured in Bit. For example, L5 has 8 Bit resolution (ranges from 0-255), while L8 has a 16 Bit (ranges from 0-65535) radiometric resolution. Lastly, the spectral resolution is the wavelength interval, or the frequency spectrum of the bands. For

example, the finer the spectral resolution, the narrower the wavelength bands or channels. L5 and L8 have multi-spectral resolution sensors with multiple bands (Table 1).

Table 1. Landsat 5 and Landsat 8 band designations, spatial and spectral resolutions.

Landsat- 5 TM- and L5 ETM+ Bands (µm)			**Landsat-8 OLI and *TIRS* bands (µm)**		
			30 m Coastal/Aerosol	(0.435-0.451)	Band 1
Band 1	30 m Blue	(0.44-0.514)	30 m Blue	(0.452- 0.512)	Band 2
Band 2	30 m Green	(0.519-0.601)	30 m Green	(0.533-0.590)	Band 3
Band 3	30 m Red	(0.631-0.692)	30 m Red	(0.636-0.673)	Band 4
Band 4	30 m NIR	(0.772-0.898)	30 m NIR	(0.851-0.879)	Band 5
Band 5	30 m SWIR-1	(1.547- 1.749)	30 m SWIR-1	(1.566-1.651)	Band 6
Band 6	60 m TIR	(10.31-12.36)	100 m TIR-1	(10.60-11.19)	Band 10
			100 m TIR-2	(11.50-12.51)	Band 11
Band 7	30 m SWIR-2	(2.064-2.345)	30 m SWIR-2	(2.107-2.294)	Band 7
Band 8	15 m Pan	(0.515-0.896)	15 m Pan	(0.503-0.676))	Band 8
			30 m Cirrus	(1.363-1.384)	Band 9

Solar energy illuminates the Earth's surface. A fraction of the energy or photons are either absorbed, transmitted, and reflected to space. Any given object on Earth's surface absorbs (the process by which radiant energy is absorbed) and reflects (the process where radiation ‘bounces off’ from the sensed object) and transmit energy. The percentage reflected, percentage absorbed, and percentage transmitted depend on the object's unique characteristics, including chemical composition, water content, heat capacity, color, surface roughness, and albedo properties. As a result, each land cover type exhibits a unique spectral response curve. Fig. 1 provides an example of four spectral profiles for different land covers.

Remote sensing technology has many applications. In this study I used it to examine the changes of urban green spaces over time, using the Visible and NIR bands (0.44- 0.89 wavelength in µm). I also use thermal infrared remote sensing (10.31-12.51 wavelength in µm) to investigate thermal emission characteristics of the land surface temperature of the urban green spaces (UGSs) over time.

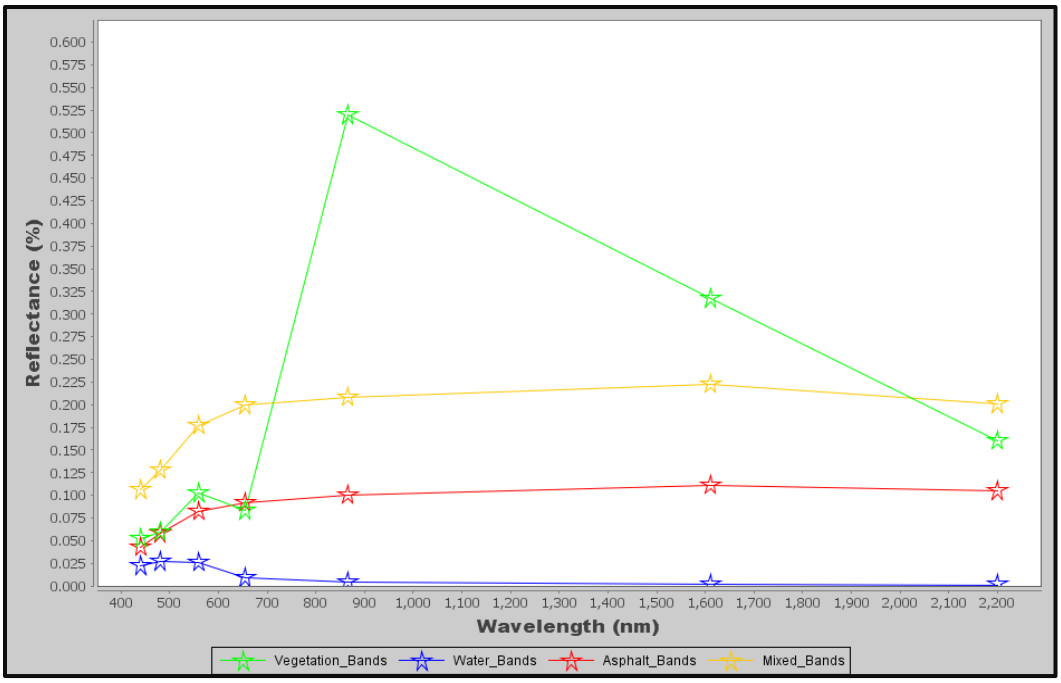

Figure 1. Spectrum profile of vegetation (green) reflects higher in the near-infrared (NIR) and low in the visible light. This is due to the cellular structure, particularly the spongy mesophyll. Water (blue) has lower reflection in visible bands, and then it drops close to 0 reflectance in other bands. Mixed surface (yellow) shows high reflectance in the visible bands and overall flat reflectance in other bands, similarly, asphalt (red) is the second lowest after water.

Normalized Difference Vegetation Index

This work examines the urban vegetation change from 1986-2019, a 33-year period. The Normalized Difference Vegetation Index (NDVI) is the most commonly used spectral index to measure the health of vegetation (Huete et al. 1985; Glen et al. 2008). NDVI is the foundation for remote sensing phenology studies. Vegetation photosynthesis allows vegetation to absorb solar energy in the (0.4 to 0.7 µm) spectral region. On the other hand, to prevent overheating, vegetation strongly reflects solar energy in the near-infrared spectrum (0.7 to 1.1 µm). To

calculate NDVI we use the spectral bands in the near-infrared (NIR) and red (RED) range of the electromagnetic spectrum, using the following formula:

$$NDVI= (NIR -RED) / (NIR + RED) \quad (1)$$

Green vegetation absorbs strongly in the red range of the electromagnetic spectrum, and reflects strongly in NIR, resulting in relatively high NDVI values. Unhealthy or senescent vegetation absorbed far less in RED and does not reflect as strongly in NIR resulting in lower NDVI values. While the theoretical range of NDVI varies from -1 to 1, most non-water/non-snow surface show NDVI values above 0, with values close to 1 indicating healthy and dense vegetation.

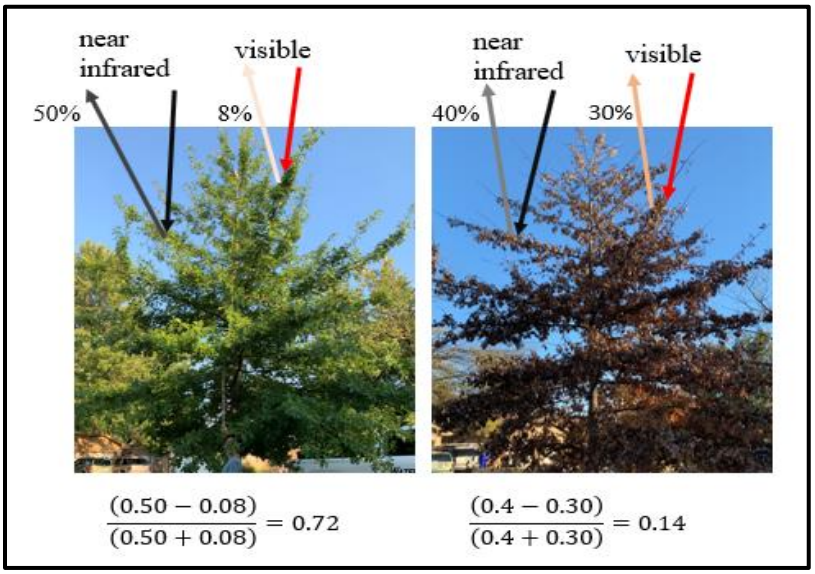

Figure 2. Example of NDVI differences for healthy and senescent vegetation

Thermal Remote Sensing

Thermal infrared remote sensing allows the sensing of previously invisible source of information, as human eyes cannot sense thermal infrared energy (3.0 – 14 μm) or radiant energy, meaning the energy emitted from an object or land surface. Thermal infrared records the apparent radiant energy rather than the true kinetic energy. Most objects (except glass) have high

kinetic energy and have high amount of radiant energy (Torgersen et al. 2001). The total radiation or exitance (M_b), measured in Watts m^{-2} is proportional to the fourth power of its temperature:

$$M_b = \sigma T^4 \quad (2)$$

where M_b is the total spectral radiant exitance, σ is the Stefan-Boltzmann constant = 5.6697 x 10^{-18} W m^{-2} K^{-4} and, T is the temperature in Kelvin.

Since earth surface cover is composed of selectively radiating bodies, for example water, rock or vegetation that emit only a portion of the energy compared to blackbody, emissivity is an important component of the full equation. A blackbody is a theoretical construct that absorbs all the solar energy and radiates energy at the maximum possible energy rate per unit area. Emissivity (ε) is the ratio between the actual radiance emitted (M_r) and the radiance of a blackbody at the same kinetic temperature (M_b) (Jacob et al. 2004), or

$$\varepsilon = \frac{Mr}{Mb} \quad (3)$$

According to Kirchhoff's law of thermal radiation, objects that are good absorbers are good emitters, and good reflectors are poor emitters. For this reason, the relationship between reflectance (r_λ) and emissivity (ε_λ) must be accounted for. Knowing the emissivity of an object makes it possible to modify the Stefan-Boltzmann law originally applicable to blackbodies, so that it pertains the total spectral radiant flux (M_r). With, $M_r = \varepsilon \sigma T_{kin}^{\ 4}$ and $T_{rad} = \varepsilon^{1/4} T_{kin}$ then,

$$\varepsilon = \left(\frac{Trad}{Tkin}\right)^4 \quad (4)$$

As indicated in Table 1, for L5 and L7 the thermal infrared band (10.31-12.36) correspond to band 6 and for L8 there are two bands 10 and 11, but only the band 10 is used as band 11 has some reported issues (Barsi et al. 2014).

Chapter 2: Multi-Temporal Land Surface Temperature and Vegetation Greenness in Urban Greenspaces of Puebla, Mexico

Gomez-Martinez F, de Beurs KM, Koch JA, Widener J, 2021. Multi-Temporal Land Surface Temperature and Vegetation Greenness in Urban Greenspaces of Puebla, Mexico. To be submitted to Land, December 2020.

2.1 Introduction

Cities are home to 55% of the world's human population, a percentage projected to increase to 68% by 2050 (UN DESA, 2018). Cities host important institutions that make policy and economic decisions. Comprised of complex systems, cities generate challenges and opportunities for the multitude of different social classes that intermingle in them. Young people searching for economic, academic, and other opportunities arrive without intending to return to rural communities, a phenomenon known as 'rural flight' (Anuja et al., 2018; Nelson & Nelson. 2011). As city populations grow, so does the rate of urbanization, resulting in environmental transformations such as replacing vegetated land covers with impervious surfaces (IS).

IS include housing, roads, parking lots, sidewalks, shopping centers, and airports. Primarily constituted of concrete and asphalt, these structures provide shelter and mobility; however, they also disrupt the ecosystems and negatively impact biodiversity (McKinney 2002). In some cases, IS prevent rainwater infiltration and inhibit groundwater regeneration. This creates water quality and quantity issues for cities located in arid regions. IS and related infrastructure can also cause flooding, as rainwater flows to lower areas (Shuster et al., 2007), resulting in economic impacts and in some instances, loss of life (Hammond et al., 2015).

Additionally, most IS materials are gray or black, which absorb more incoming solar energy than vegetated land surfaces. These materials also have a high-heat storage capacity that delays energy emission. In tropical countries and especially during the summer seasons, IS

increase heat storage (Santamouris et al. 2015). Tropical countries receive more shortwave radiation or insolation from the sun. They are located around the equator line between the Tropics of Capricorn and Cancer. Examples of hot countries include Australia, India, Indonesia, and Mexico. When urban temperatures rise, increase in energy use related to cooling systems further warms these cities (Polydoros & Cartalis, 2015).

The term Urban Heat Island (UHI) refers to higher temperatures in cities compared to surrounding rural areas not impacted by urbanization (Zhao et al. 2018; Liu et al. 2018; Maimaitiyiming et al. 2014; Voogt & Oke, 2003). These temperature differences can range from small increases of 0.6°C to extremes of 12°C (Yague et al. 1991; Rosenzweig et al. 2005; Vidrih & Medved, 2013). The high variability of UHI stems from each city's unique characteristics of urbanization, climate zone, land cover types, latitude, elevation, prevailing wind directions, and the surrounding land cover context (Zhang et al. 2017). Regardless of the unique characteristics each city presents, Li et al. (2017) argue that the processes of urbanization can explain up to 87% of UHIs, especially in cities surrounded by homogenous vegetation cover.

Urban heat was first examined in the city of London using atmospheric temperature data from weather stations (Howard, 1818). Much later Rao (1972) used remotely sensed data to investigate the land surface temperature. Oke (1982) investigated both short-wave and long-wave radiation fluxes in cities in comparison with surrounding rural areas. UHIs have since been examined across the seasons, with most of the literature concluding this phenomenon reaches its peak during summer months (Zurita & Martinez, 1991; Ren et al., 2007; Yuan & Bauer, 2007; Hamada & Otha 2010; Ren et al. 2013). Studies demonstrate that the substitution of vegetation in any climate with manufactured structures is the primary driver of UHIs because flora generally

provide evapotranspiration (Hamilton et al. 2017; Hanson, 1991) and higher albedo, except for cacti and other succulent plants (Trlica et al. 2017).

UHI studies illustrate how urbanization and UGSs have a negative correlation (Ren et al., 2007; Maimaitiyiming et al. 2014). UGS generate 'cooling islands' that can potentially reduce or mitigate an UHI (Lin et al. 2015), especially in the case of big parks with healthy canopies (Chang & Li, 2014). The cooling capacity of UGS directly relates to the size, shape and intensity of the green space itself (Zhang et al. 2017). While green strips or small parks do not have the same cooling capacity as big parks, it remains critical to examine their impacts because they still provide recreational activities, shade, and serve as meeting points (Zhang & Zhou, 2018). UGS provide ample economic and social benefits as well as other ecosystem services (von Döhren & Haase, 2015).

In this study I examine the vegetation changes of UGS and their relationship to LST over time in the Mexican city of Puebla. I begin with a brief overview of the literature examining UHI in Mexico, an understudied region. Next, we analyze NDVI to determine the transient nature of UGS in Puebla over the course of 33-years. Finally, we document the unique characteristics and circumstances of 80 UGS in the city with in-depth field observations.

2.1.1. Geographic biases of UHI studies

Starting in 2005, the number of peer-review publications focused on UHI increased exponentially; this burst of scholarship has resulted in geographic asymmetries regarding cities being studied (Zhou et al. 2018). A literature review by Zhou et al. (2018) indicates that UHI studies and the use of remotely sensed data have largely focused on five large Chinese cities (213), a small selection of cities in the USA (106), two cities in India (38), as well as a few other

cities: Berlin (11), Paris (11), São Paulo (5), Lagos and Sydney (4 each). While there may be underlying reasons contributing to this research imbalance, it is important to study a wider range of cities to understand UHI impacts. This type of analysis is particularly important for cities where informal settlements occur, as is the case in Latin America, where urban green infrastructure is often sparse (Roberts et al. 2017; Arocena & Senker, 2016; Alcorta & Perez, 1998). Limited investment in education and technology in less developed cities (Moguillansky, 2016; Eakin & Lemos, 2006), in tandem with global disruptions such as climate change and pandemics, further exacerbate social and environmental vulnerabilities as is the case in the cities of Mexico.

Along with Mexico City (with over 8 million people), ten other cities in Mexico had populations of 1 to 2 million people in 2010 (INEGI, 2010). The few UHI studies undertaken in Mexico have primarily focused on Mexico City, with one study exploring how urban morphology influences solar and radiative exchanges (Jaregui, 1993), and others examining the role of canopy cover on UHI mitigation (Ballinas & Barradas, 2015; Cui & de Foy, 2012). Rivera et al. (2017) reveal how soil wetness weakens UHI effects and how wind-flow affects the spatial distribution of UHI in the metropolitan area of Toluca. Jauregui et al. (1992) illustrate how urbanization positively correlates with rising temperatures in Guadalajara; Villanueva-Solis (2017) does the same for Mexicali. The only study of UHI in Puebla uses atmospheric temperature data to document temperature differences in the city's historic center, as well as strategic areas with heavy traffic concentration (Abarca et al. 2019). Our work uses optical and thermal remote sensing to identify UHI and their relationship with UGS and treats UGS as impermanent and constantly evolving spaces.

2.1.2. Temporal Dynamics of UGS

Many UHI studies treat UGS as static. Few studies address the dynamic nature of vegetation cover resulting from aging, climatic, or human-induced transformations. One exception is Mackey et al. (2012). These authors observed vegetation and reflective surface changes from 1995 - 2009 in the city of Chicago by examining NDVI, albedo, and temperature changes of UGS and their positive/negative correlations with LST (Mackey et al., 2012). Another exception is Glenn et al. (2008), who highlight how UGS experience physiological stages differently within the same city. Similarly, others have found that vegetation cover types differ within a park, and from park to park (Glenn et al., 2008). Attentive to this variability across time and space, our study examines 33 years of data for 80 UGS, examining their spectral signatures and the relationship between green vegetation and land surface temperature.

2.1.3. Importance of field observation

Remotely sensed data undoubtedly enables the examination of human impacts on land cover change from a distance. Studies exclusively relying on remotely sensed data, however, have shortcomings. For instance, passive remotely sensed data such as from Landsat sensors depend on solar radiation and cloud-free days in order to detect urban land cover signatures. Satellite data also depend on temporal and spatial resolutions (Zhou et al. 2019). For example, optical data from Landsat 5, 7 and 8 used in this study have a spatial resolution of 30 meters, while thermal bands for L5 and L7 (band 6) have 60 m resolution, and thermal bands for L8 (bands 10 and 11) have 100m spatial resolution. While land cover heterogeneities exist in a 900 m^2 area (30mx30m pixel), it is difficult to account for land cover variability in mixed pixels. Even if a certain pixel consists of the same type of vegetation, other areas of the park might have

different vegetation types. It is, therefore, important to ground truth satellite observations by performing field inspections of study area.

While some studies featuring in-situ observations have focused on the potential health and economic benefits that UGS provide, they have not explored vegetation cover differences from one park to another park. A survey in the Chinese city of Guangzhou revealed that many park users believe that UGS mitigate poor air quality and contribute to the well-being of visitors. This survey also found that higher educated people generally perceived parks more favorably (Duan et al., 2018). Similarly, Gibson (2018) indicates that older adults experience autonomy and fulfillment when visiting city parks. UGS enable positive health outcomes (Kondo et al., 2018), add recreational value (Zhang & Zhou, 2018), and contribute to overall well-being of park users (Kothencz et al. 2017). Sherer (2006) notes that UGS increase property values and attract businesses and tourists. In addition to the use of satellite derived data, we visually evaluated 73, out of the 80 UGS sites in our study in order to determine land cover characteristics and dominant vegetation species, as well as the level of maintenance a park received, and services found within it.

2.2. Study Area

Puebla is the largest city in, and capital of, the Mexican state of Puebla (Fig. 3). During the colonial period of Mexico, this city was known as 'Puebla de Los Ángeles,' after independence it became 'Heroica Puebla de Zaragoza;' here we simply refer to the city as Puebla. In 2010, Puebla was the fourth largest city in Mexico. The most recent demographic data from the National Institute of Statistics and Geography (INEGI), a 2015 intercensal survey, indicates it was home to 1,579,259 people. Puebla's population has grown substantially (82%)

between 1980 and 2010 (Fig. 4) due to immigration of people from peripheral areas. The population growth has been accompanied by significant urbanization which is easily visible on Landsat imagery from 1986 and 2019 (Fig. 5).

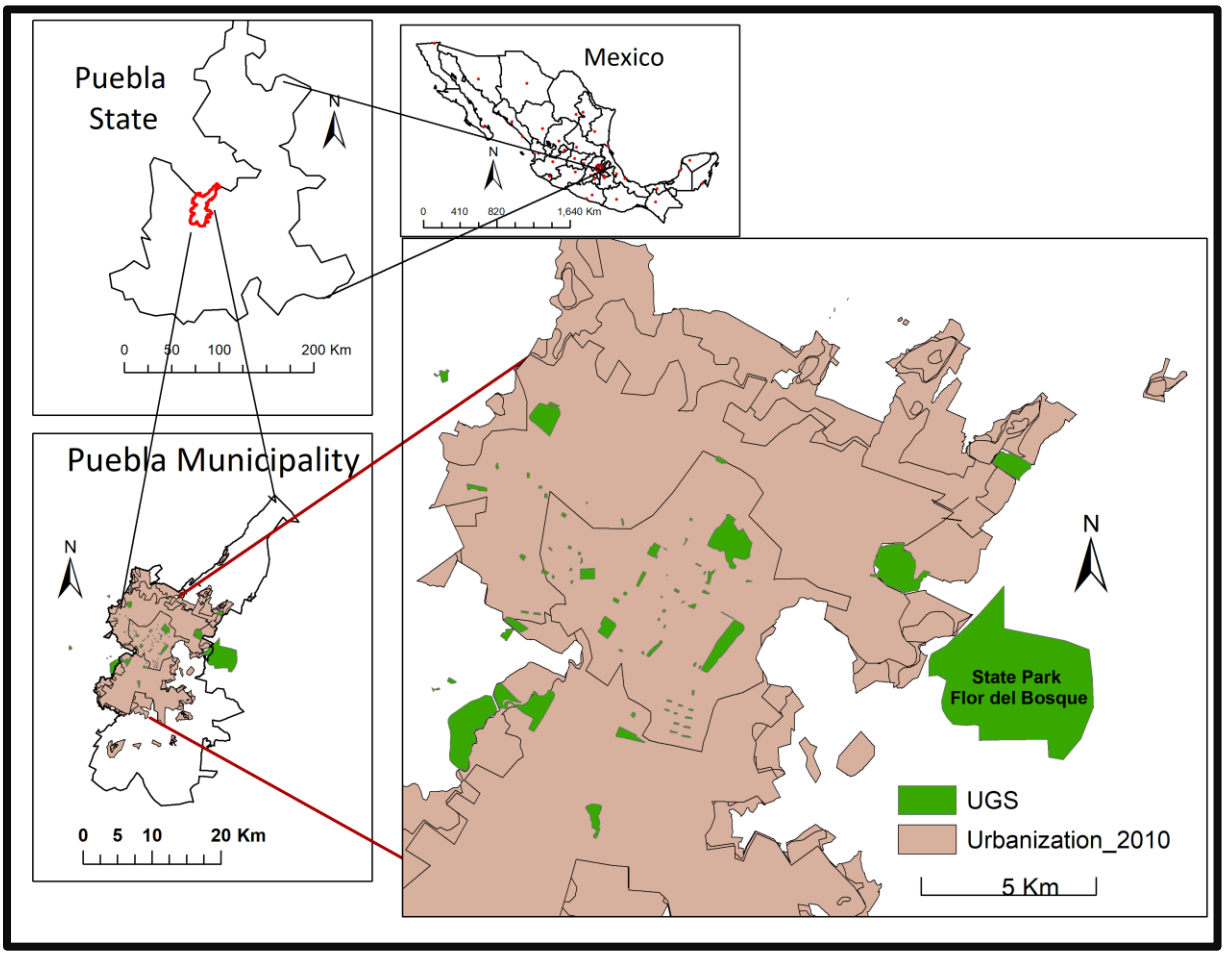

Figure 3. Location of Puebla, its 2010 urban extend and 80 urban green spaces (UGS). These UGS are mostly public parks, but also include five cemeteries, one golf course, three neighborhoods, and a state park: Flor del Bosque with the size of (13,404, 500 m^2)

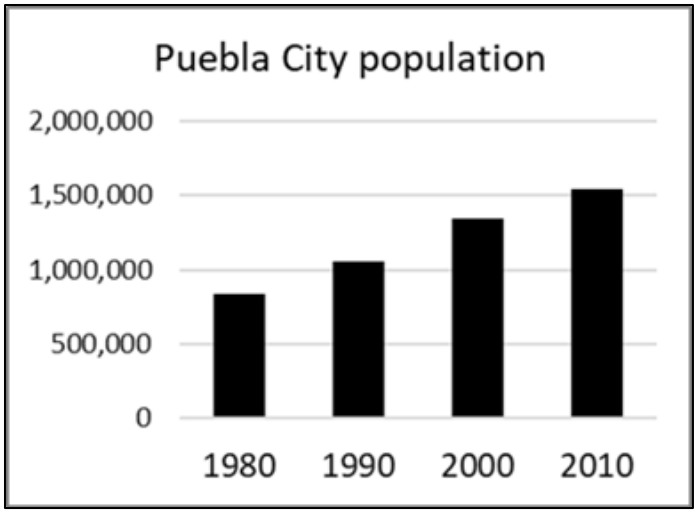

Figure 4. Puebla's experienced an 84.2% population increase between 1980 and 2010.

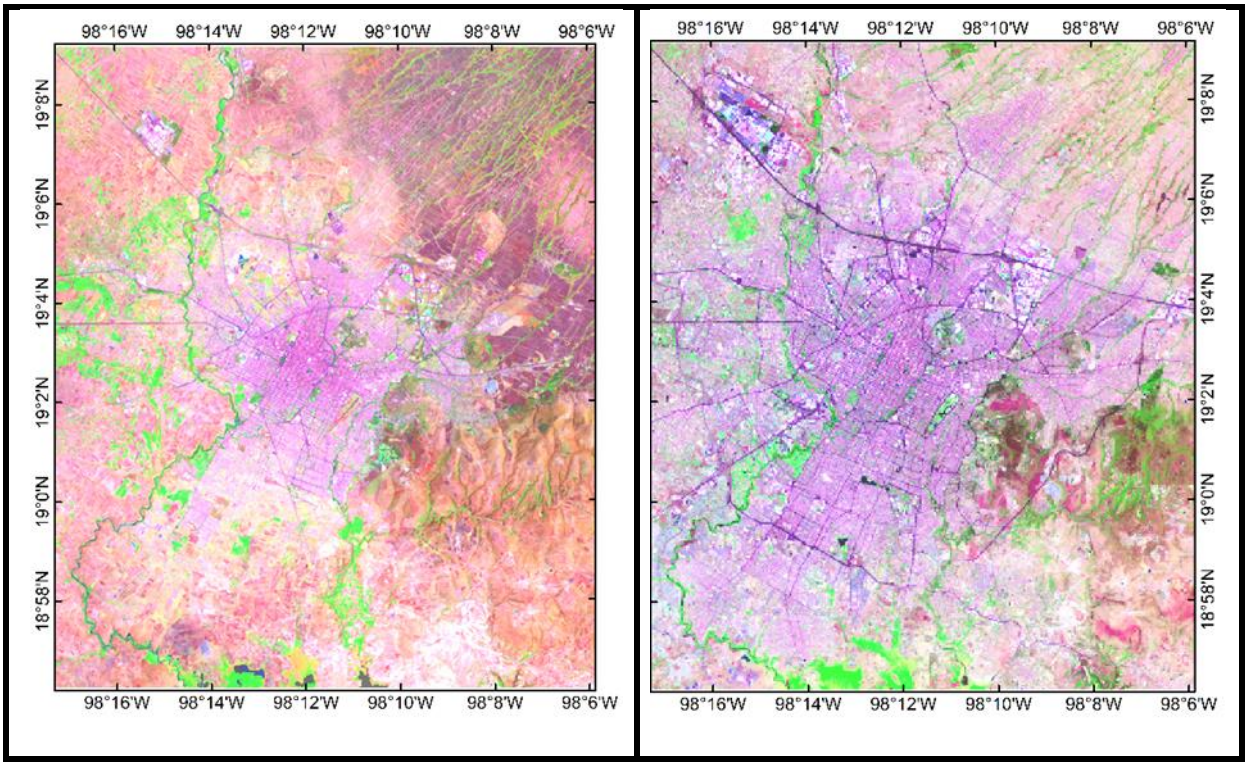

Figure 5. A 33-year comparison of urbanization from May 3,1986 using Landsat 5 data, RGB band combination (5,4,3) on the left, and May 14, 2019 using Landsat 8, band combination (6,5,4) on the right.

Puebla is characterized by a subtropical highland climate according to the Köppen climate classification. Spring weather is dry and warm, summers are hot and wet, autumn weather is mildly cold and dry, and winters are cold and dry (Abarca et al. 2019). Puebla includes 53,432 km^2 in area with an elevation of 2,135 m (7,005 ft.). May is the warmest month with an average temperature of 28^{o}C (82.4^{o}F) and the highest recorded temperature of 35.5^{o}C (97.7^{o}F). According to Mexico's National Meteorological service, Puebla's yearly precipitation average is 970 mm (38.15 inches). Located within the Trans-Mexican Volcanic Belt, which spans the Pacific coast to the Gulf coast (Eisenstadt, 2019; Barton 2019), Puebla is surrounded by three volcanoes: Popocatepetl, Ixtaccihuatl, and La Malinche. Popocatepetl remains active, spewing volcanic gas multiple times a year and showering the city and neighboring towns with ash and dust particles. The city also regularly experiences earthquakes of varying sizes, the latest major earthquake with a magnitude of 7.1 (M_w) and a duration of ~20 seconds, occurred on September 19th, 2017 (National Seismological Service of Mexico, 2017).

2.3. Data

Our study relies on data from Landsat 5 Thematic Mapper (L5 TM), Landsat 7 Enhanced Thematic Mapper (L7 ETM+) and Landsat 8 Operational Land Imager (OLI) & Thermal Infrared Sensors (TIRS) with a slight variation in band designations. L5 and L7 have a total of eight bands, including a panchromatic and thermal band. L8 features eleven bands, the same as L5 and L7 plus coastal aerosol, cirrus, and two thermal bands: 10 and 11. We selected two Landsat tiles: path 26 row 47 and path 25 row 47 and processed all data on the Google Earth Engine. We have chosen the month of May to acquire consistent data from 1986 to 2019. We applied a filter of < 20% cloud cover, applied a cloud mask, and then visually inspected each tile

individually to ensure the study area was free of clouds (Table 1). We did not calculate land surface temperature (LST) for the first four images from May 03, 1986 to May 04, 1998 because the data necessary for the atmospheric correction are only available from January 19, 2000 (https://atmcorr.gsfc.nasa.gov/).

Table 2. Landsat products used, sensors types and respective dates.

Sensor	***Date***	***Sensor***	***Date***	***Sensor***	***Date***	***Sensor***	***Date***
L5	*May 03, 1986*	*L7*	*May 01, 2000*	*L8*	*May 16, 2014*	*L8*	*May 18, 2018*
L5	*May 22, 1993*	*L5*	*May 09, 2000*	*L8*	*May 19, 2015*	*L8*	*May 27, 2018*
L5	*May 14, 1996*	*L5*	*May 28, 2001*	*L8*	*May 28, 2016*	*L8*	*May 14, 2019*
L5	*May 04, 1998*	*L5*	*May 24, 2011*	*L8*	*May 08, 2017*	*L8*	*May 21, 2019*

A shapefile of Puebla's city limit was acquired from the Municipal Planning Institute of Puebla (IMPLAN, http://implan.pueblacapital.gob.mx/) and the shapefiles of the state and country were downloaded from INEGI site (https://www.inegi.org.mx/app/areasgeograficas/?ag=21).

2.4. Methods

2.4.1. UGS identification and their digitized boundaries

To determine Puebla's urban green spaces (UGSs), we consulted an inventory of green areas prepared by the municipal government. This inventory listed a street address and coordinate for each green space, but it did not provide names or spatial vector data. We selected 80 UGSs using Google Maps. All 80 UGSs polygons were manually digitized using Google Earth, zooming in 200 m, then saved as Keyhole Markup Language Zipped (KMZ) file. Then, that KMZ file was opened in ArcMap and saved as a shapefile.

During the months of March, April and early May of 2018, we visited 73 of the 80 selected UGS to corroborate their names and visually inspect land cover types and other

characteristics. To conduct this fieldwork, we relied on a bike share system and the Red Urbana de Transporte Articulado (RUTA), a metrobus system. Locations not accessible through public transportation were reached with the help with a family friend with a car, or by relying on the ride share service Uber.

Our selection of 80 UGS features 68 parks that ranged from 743 m^2 to 1,563,180 m^2 in size. Some were lacking amenities, while five were recently completed large and carefully landscaped tracts of land featuring high end restaurants, museums and other attractions, as well as a range of recreational equipment and program activities. Five of the selected UGS were cemeteries distinguished by significant greenery compared to their surroundings. Three others, which we call "neighborhood cases," Case-1 (496,869 m^2) developed in late 1970s, Case-2 (1,563,180 m^2) developed in the early 2000s, both include neighborhood golf courses, and Case-3 (17,619 m^2) is a block-sized private compound with a large swimming pool and dense Indian Laurel trees (*Ficus microcarpa*). Finally, four UGS consist of an untended strip of land covered with vegetation, a university campus, a private golf course, and a state park called Flor del Bosque (13,404,500 m^2). We selected these diverse UGS because they exhibit significant vegetation cover compared to their immediate surroundings. This sharp juxtaposition allowed us to examine whether these locations influence the city's microclimate. Close examination of characteristics of each of the 73 UGS visited also resulted in the collection of about 450 photographs to capture unique attributes of UGS (e.g. Fig. 6).

Figure 6. Date Palm and Indian Laurel trees in the Zocalo park of Puebla (upper left), Eucalyptus trees in Amalucan Hill park (upper right), grass in La Constancia/Paseo de Los Gigantes or 'model park' (bottom left), and blossoming Jacaranda trees in Federico Escobedo park (bottom right).

The dominant vegetation cover of our UGS includes trees, such as Indian Laurel, Jacaranda, Eucalyptus, Bougainvillea, Pirul or Peruvian peppertree (Schinus mole), Pine trees, Date Palm, grass and other ornamental shrubs. Indian Laurel trees are one of the most distinctive tree species found in Puebla. For example, Puebla's main plaza, or Zocalo, is distinguished by giant Indian Laurel trees (Fig. 6). These trees are angiosperm or seed producing, with

oblanceolate leaves and light-gray bark. They grow as tall as 33.5 meters (110 feet) and stand out as the greenest trees, with dense canopy cover year around. Their native location ranges from tropical Asia to Australia. Over time, Indian Laurel trees have been widely distributed as ornamental trees in warm climate cities, for shade, carbon storage, and many other environmental services. Indian Laurel trees are now also found in Florida, and parts of Mesoamerica and South America. Other land covers in the selected UGS include concrete from sidewalks, buildings and two parks with significant waterbodies.

2.4.2. Normalized Difference Vegetation Index Analysis

To investigate the vegetation in each UGS over time, we calculated the Normalized Difference Vegetation Index (NDVI) for each of the 16 Landsat images. NDVI is the most commonly and widely used index in environmental studies, agricultural monitoring, and examinations of vegetation vitality changes (Rouse et al., 1973, Tucker, 1979). NDVI quantifies vegetation health indicating strong correlation with areas covered with green biomass. It can be calculated using just two bands, the RED band (0.64 – 0.67 µm) and the near-infrared (NIR) band (0.85-88 µm). NDVI is calculated using the following equation:

$$NDVI = (NIR - RED) / (NIR + RED) \quad (5)$$

The Red band measures the absorption of chlorophyll pigments signaling low reflectance, and the NIR-band senses the maximum reflection of the cell structures in leaves (Baret & Guyot, 1991). NDVI values typically range from -1 to +1. Values closer to 0 indicate absence or sparse vegetation, stress or drought, as vegetation health and canopy layers and density increase, NDVI increases reaching closer to +1 (Huete et al. 1985).

To evaluate the change of each park over the 33 years of the study period, and to avoid outlier issues as a result of weather events, normalization of the data was performed using the standard z score as follows:

$$Z = \frac{x - \mu}{\sigma} \tag{6}$$

in where the x = mean NDVI value of each park per each date, μ = mean NDVI value of all parks for each date, and σ = standard deviation of all parks by each corresponding date.

The z-score indicates the standard deviation or change of each of the UGS from the mean of NDVI of all data across all UGS. As a result, we can evaluate for each UGS whether it is greener or browner than all other parks observed for a particular image without worrying about NDVI fluctuations affecting all parks as a result of weather. We apply a linear regression of the z-scores against time and calculated the slope, adjusted R-squared, and P-values. With the slope we calculated and mapped the yearly changes of each UGS. Also, we examined the 33-year z-score changes for each of the 80 UGS, by using May 3rd, 1986 data z-score against the May 21st, 2019 z-score.

To further examine how the land cover impacted UGS changes, we grouped the UGS into categories by dominant land cover type, size, and by level of maintenance or human intervention. We formulated the following hypothesis:

Hypothesis-1: (H_o) states that UGS with Indian Laurel tree vegetation cover change at a similar rate of change of NDVI as all other UGS. (H_a) states Indian Laurel trees influence how the parks changed over time. We selected seven UGS with Indian Laurel trees as their dominant vegetation cover; five are parks (Paseo Bravo, Benito Juarez, Los Enamorados, Zocalo, Paseo de San Francisco), and the other two consist of a University campus and Neighborhood Case-3. The selection of these seven UGS is based on visual examination during field work. To address

Hypothesis-1, a *t*-test was performed comparing the rate of the change of NDVI of the seven UGS against the rate of the change of the remaining 73 UGS with mixed vegetation cover.

Similarly, we wanted to evaluate if big UGS changed in NDVI more significantly than small UGS. To examine, *Hypothesis-2* was formulated: (H_0) states that the size of UGS does not significantly influence the rate of change, while (H_a) states that the size of the UGS does influence how the vegetation greenness changed over the 33-year period. To carry out the *Hypothesis-2*, we applied a log linear regression of the rate of NDVI change against the size of the UGS.

Lastly, we examine whether the maintenance level an UGS receives influences the rate of vegetation change in greenness as measured with NDVI. For this, we formulated *Hypothesis-3* with: (H_0) stating that maintenance of UGS do not influence significant change in NDVI, while (H_a) states that the maintenance level an UGS receives does influence change. To carry out this examination, 11 UGS were identified as highly maintained and well-tended. Again, this selection is based on multiple visits to those parks in which landscape personnel were actively tending to those UGS. Of the eleven UGS, ten are parks (El Tamborcito, Los Fuertes, Cerro Amalucan, El Centenario/Chapulco Lake, Paseo de Los Gigantes, La Ninez, Jardin del Arte, Paseo de San Francisco, Ecopark Mexican Revolution, and Ecopark Metropolitano of Puebla), and the other one is a Golf Course. In this analysis, we used a two-sample t-test assuming unequal variances.

2.4.3. Land Surface Temperature Retrieval

Three methods are commonly used in the retrieval of Land Surface Temperature (LST) from thermal bands: The Mono Window Algorithm (Qin et al. 2001), the Single Channel Method (Jimenez-Munoz & Sobrino, 2003), and the Radiative Transfer Equation (RTE) (Berk et al.

1989; Qiang, Fu, 2006; A. Sekertekin, 2019). We decided to use the RTE method because it estimates specific surface emissivity, atmospheric transmittance, upwelling radiance and downwelling radiance of a given band (Li et al. 2013). Furthermore, Windahl & de Beurs (2016) conclude that the RTE method provides the lowest errors of LST calculation compared to the other two methods over an urban landscape in Oklahoma. Regardless of which of the three-retrieval method is chosen, all methods require pre-processing to calculate LST (Tang et al. 2014). We excluded four images, all before the year 2000 (see, Table 2), from the atmospheric correction process, as there are no atmospheric profiles available before 2000 (https://atmcorr.gsfc.nasa.gov/). These date exclusions yield 12 data sets from 2000 to 2019.

Land Surface Emissivity (LSE) measures the ability of the land surface to emit thermal radiation. LSE is a crucial component in the study of climatic, ecological and biochemical processes observations as well as in many other applications (Tang & Li, 2014). LSE reveals characteristics of surface top layer such as soil or vegetation as well as unevenness of the surface (Sobrino et al., 2008; Li et al., 2013).

Similar to LST retrieval methods, currently, three methods exist that are commonly used to calculate LSE: classification-based emissivity (Perez & DaCamara, 2005), day/night temperature-independent spectral-indices (Wan & Li, 1997), and the NDVI method (Griend & Owe, 1993). In this study we use the classification-based emissivity of ASTER Global Emissivity Dataset (ASTER GED) at 100m spatial resolution (Hulley et al. 2015, & Hulley and Hook, 2009), then applied the monthly adjustment to adapt the emissivity to correct for bare ground and vegetation based on the NDVI layer delivered with the dataset.

To atmospherically correct the thermal bands, we first calculate the blackbody radiance at ground-level as follows:

$$B_*(Ts) = \frac{L_* - (1-\varepsilon_6)\tau_* L_*^{\downarrow} - L_*^{\uparrow}}{\varepsilon_* \tau_*} \quad (7),$$

where * is the Landsat band number, e.g. 6 as in Band 6 for Landsat 5 and 7 and $\varepsilon_*$is calculated based on the Aster Global Emissivity Dataset. Where L_* is the top-of-atmosphere radiance ($W\ m^{-2} sr^{-1} \mu m^{-1}$) of the Landsat (5,7,8) thermal bands. τ_* is the atmospheric transmittance retrieved from the Atmospheric Correction Parameter Calculator. $L_*^{\uparrow}$is the upwelling radiance ($W\ m^{-2} sr^{-1} \mu m^{-1}$) retrieved from the Atmospheric Correction Parameter Calculator. $L_*^{\downarrow}$is the downwelling radiance ($W\ m^{-2} sr^{-1} \mu m^{-1}$) retrieved from the Atmospheric Correction Parameter Calculator. The inverse of the Planck function was used to calculate LST (K) from the surface blackbody radiance (Chander et al. 2009):

$$T_S = \frac{K_2}{ln\left(\frac{K_1}{B_*(T_S)} + 1\right)} \quad (8),$$

where the constants K1 and K2 are derived from the Landsat metadata, and B* is derived in (7).

2.4.4. Statistical analysis of LST data

After retrieving LST from the thermal bands of the 12 satellite images, mean values of LST were extracted for each of the UGS. We then calculated the z-score to standardize the LST values across all datasets for each of the UGS, using the Equation 6. We applied ordinary least squares regression to the z-scores against time to calculate the slope, p-value, and adjusted R square for each of the 80 UGS.

Hypothesis-1 was formulated: (H_0) states that the size of UGS does not significantly influence the LST mean z-score, while (H_a) states that the size of the UGS does influence LST mean z-score. To carry out the *Hypothesis-1*, we applied a log linear regression of the LST mean z-score of LST against the size of the UGS. *Hypothesis-2* was formulated: (H_0) states that the

size of UGS does not significantly influence the rate of LST, while (H_a) states that the size of the UGS does influence LST over the 19-year period. To carry out the *Hypothesis-2*, we applied a log linear regression of the rate of LST change against the size of the UGS. Lastly, we plotted the LST z-scores against the z-scores from NDVI to examine the relationship between park greenness and park temperature over time using the data for year May 1st, 2000, May 24th, 2011 and May 21st, 2019.

2.5. Results

2.5.1. Results of NDVI Analysis

After calculating the mean NDVI for each of the 80 UGS across the 16 Landsat images, we combined all the NDVI values from all the parks by each year to examine the yearly trend (Fig 7). The NDVI for all the parks is increasing slightly over time ($p<0.02$), with significant variation from year to year as. Similarly, we plotted the standard deviation of the 80 UGS for each year (Fig. 8). The standard deviation also increased slightly over time ($p<0.04$).

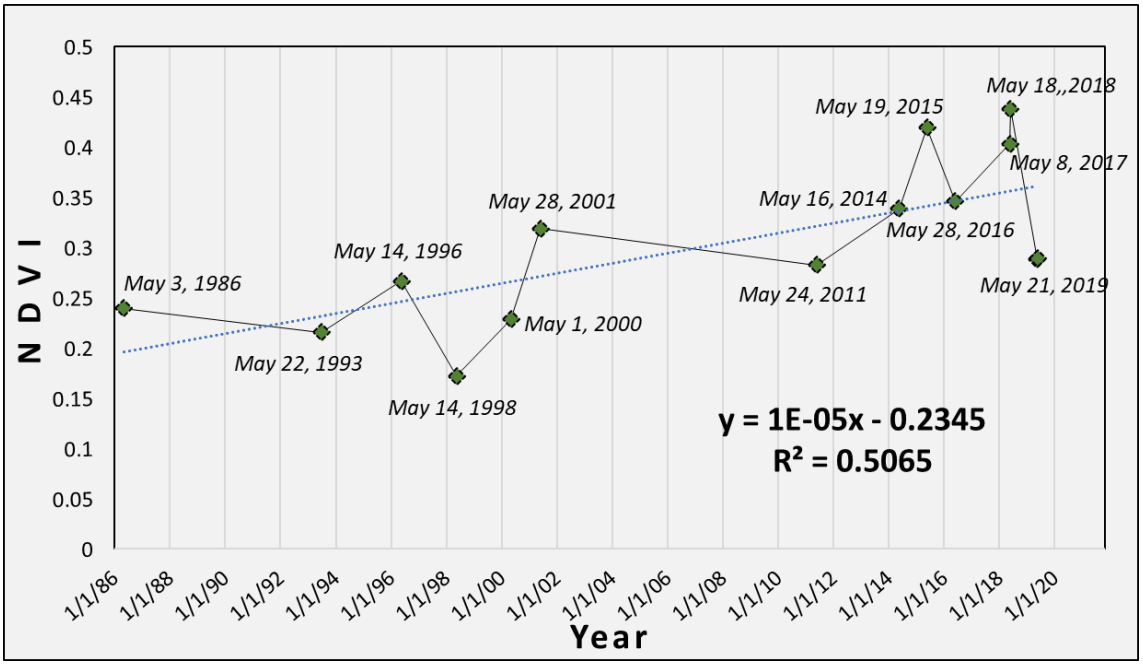

Figure 7. Yearly NDVI mean across the 80 UGSs

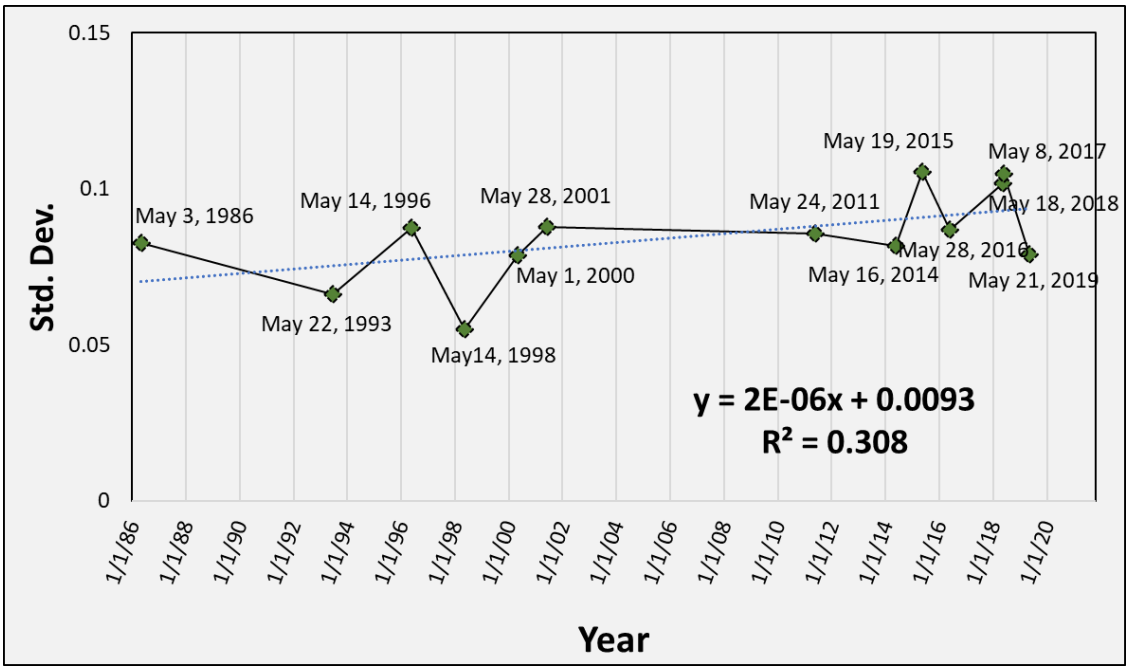

Figure 8. Yearly standard deviation from the 80 UGSs

2.5.2. Yearly UGS Changes

Figure 9 provides a visual summary of the z-score changes for each of the 80 UGS. We found two parks with significantly browning ($p<0.02$): El Centenario/Lake Chapulco and La Luna. Twenty-six UGS showed moderate browning ($p<0.05$), thirty UGS revealed No Change, eighteen revealed moderate greening ($p<0.05$) and four revealed significant greening ($p<0.02$). The four UGS with significant greening were Neighborhood Case-2, Jardin del Arte, Paseo de San Francisco and the Soccer Field.

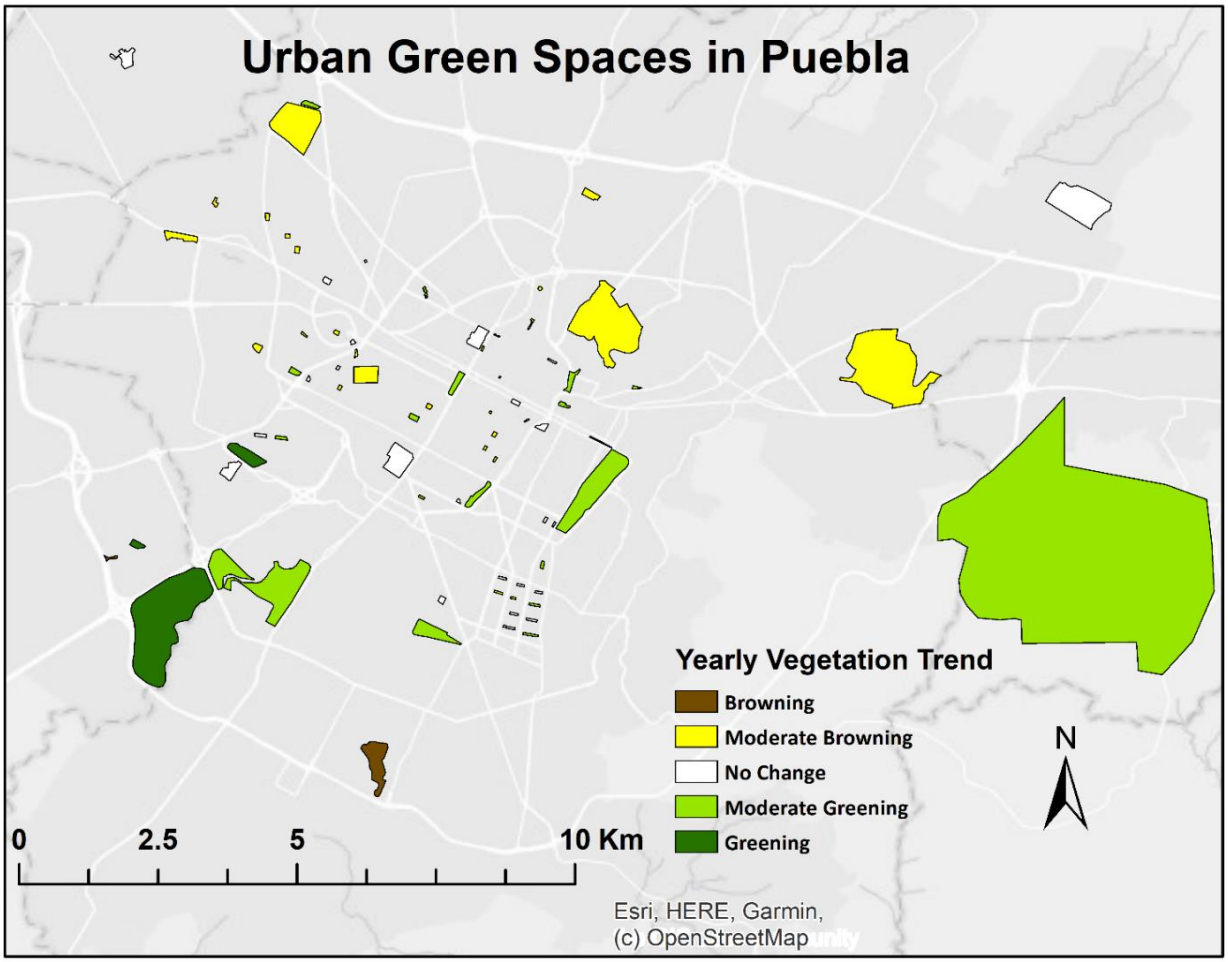

Figure 9. Visual summary of the yearly changes of each of the 80 UGSs during the 33-year period of this study.

2.5.3. Thirty-three-year comparison of changes in positive and negative direction.

In an effort to understand how each of the 80 UGS changed over time, we compared the z-score of the 37 UGS that had a positive z-score in 1986, meaning they were greener than average, against their z-score in 2019 (Fig. 10). UGS de Santa Cruz had the highest z-score in 1986; this park was almost three standard deviations greener than the average park in 1986. During the 33-year period the z-score of UGS de Santa Cruz declined to ~1.8, still much greener than the average UGS. We visited UGS de Santa Cruz and determined that the declining z-score of this UGS might be attributed to the reduction of canopy density, this UGS is dominated by eucalyptus trees, with many of the trees going through senescence.

The Golf Club showed the second highest z-score in 1986, which remained relatively stable, when compared with its z-score in 2019. The relative consistency of this z-score is likely the result of human intervention. This private Golf Club is heavily maintained and irrigated. Three parks, Villa ATL (500,736 m^2), Cerro Amalucan (1,350,060 m^2) and State park Flor del Bosque (13,404,500 m^2), also remained consistent during this study period, despite minimal maintenance. The 33-year consistency in these three parks might be due to their vegetation and location; the vegetation cover of these three UGS is mainly dominated by trees, and other vegetation types that thrive in Puebla's climate. In addition, they are relatively removed from the city core, which reduces human impact. However, as Puebla's population increases, more human disruption is starting to occur. For example, in the state park Flor del Bosque, camping, hiking and other recreational activities are now being developed. Similarly, in El Cerro Amalucan park a large public swimming pool and dozens of studio rooms were inaugurated in 2020.

Of the three parks with the smallest positive z-scores in 1986, El Cri Cri (3009 m^2) experienced vegetation loss ~ -0.8, Amanda (4273 m^2) remained relatively stable, and Strip-3 (5243 m^2) experienced vegetation loss as well (~ -0.5 in 2019). Park Amanda has the most tree canopy and other vegetation cover compared to the other two parks, while the other two have some shrubs but also significant concrete surfaces. Out of all 37 UGS, La Luna park experienced the greatest loss in greenness, going from much greener than average in 1986 to much browner than average in 2019. During our field inspection, we found that La Luna is a relatively new park; before becoming a park, it was an empty lot covered with vegetation. When the lot became a park, its native vegetation was replaced with gravel, cacti and other arid succulent vegetation. Similarly, the Soccer Field was an empty lot in 1986, which was converted to a soccer field by the Universidad Popular Autonoma del Estado de Puebla (UPAEP). During the conversion, grasses were planted, and an irrigation system was installed. As a result, it experienced the strongest increase in greenness ~ 1.5 between 1986 and 2019. Los Enamorados park which is covered mostly with Indian Laurel trees, which have increased significantly in canopy area and density, also shows a significant increase in greenness.

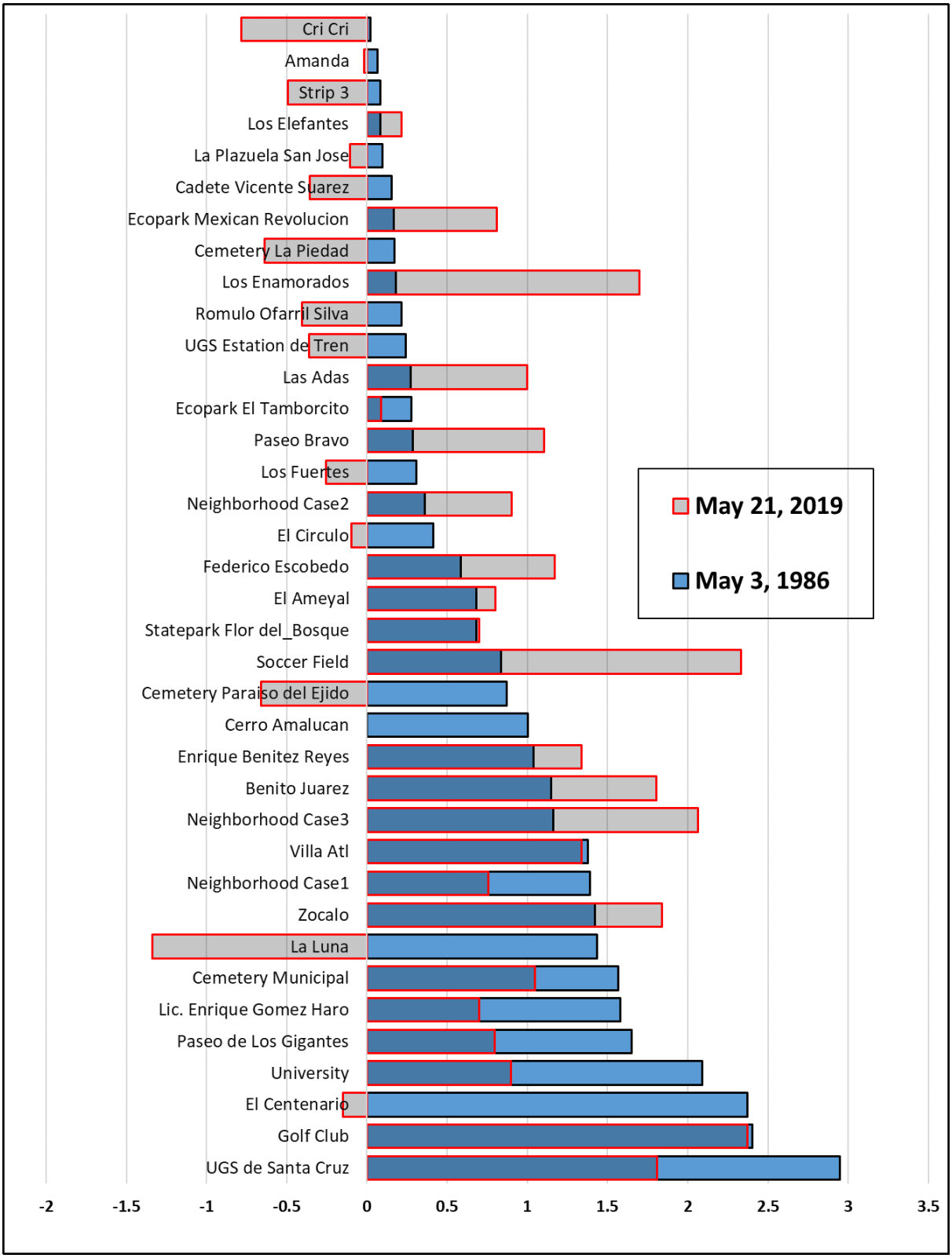

Figure 10. 37 UGS with positive z-scores on May 3, 1986 compared with their z-scores on May 21, 2019.

We also investigated the 43 UGS that had a negative z-score in 1986 (Fig. 11). There are only six parks that converted from being browner than average in 1986, to becoming greener than average in 2019: Paseo San Francisco, Ecopark Metropolitano of Puebla, 2 de Octubre, Jardin del Arte, Jardines Paseo de San Francisco and Las Ninjas. Out of the six, Paseo San Francisco increased the most from -.05 in 1986 to 1.9 in 2019. Also, it is important to mention that these three parks (Ecopark Metropolitano de Puebla, Paseo San Francisco, and Jardin del Arte) experienced major renovation and vegetation cover was expanded during the administration of Rafael Moreno Valle Rosas as state governor of Puebla from 2011 to 2017. There were twenty UGS that were already browner than average in 1986, that experienced further loss in vegetation cover.

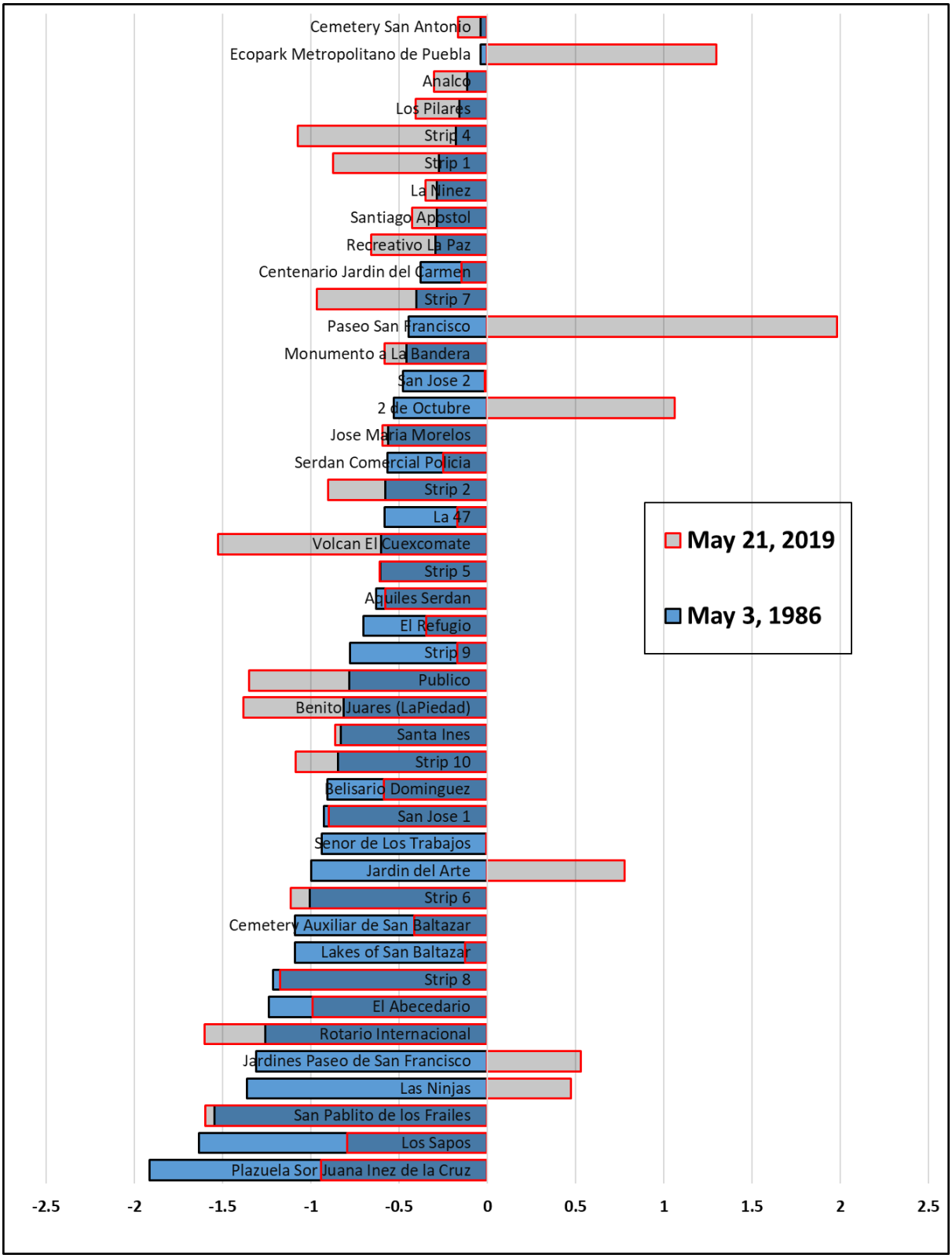

Figure 11. 43 Urban green spaces (UGS) with negative z-scores on May 3, 1986 compared with their z-scores in May 21, 2019.

2.5.4. Hypothesis Testing of NDVI

To better understand the impact of Indian Laurel vegetation cover, UGS size, and UGS maintenance on greenness of the UGS we present a series of hypothesis test results (see section 2.4.2).

2.5.4.1. UGS with Indian Laurel vegetation cover case study

To test whether UGS dominated by Indian Laurel vegetation changed more significantly than UGS with other mixed vegetation types, we compared the slope of the regression line of the z-scores against years. We identified 7 UGS which were dominated by Indian Laurel and compared their regression slopes against 73 UGS with mixed vegetation cover. We would expect that the average rate of the change for the z-scores from the UGS with mixed vegetation cover would be approximately 0, which we indeed found (Table 3). However, the t-test results indicate that there is no significant difference (p= 0.30) between the rate of change of UGS with mixed vegetation cover and the UGS with Indian Laurel tree vegetation cover.

Table 3. t-test of Indian Laurel against mixed vegetation cover.

t-Test: Two-Sample Assuming Unequal Variances		
	mixed cover	***Indian Laurel cover***
Mean	-1.877E-06	0.000035
Variance	4.412E-09	7.21633E-09
Observations	73	7
Hypothesized Mean Difference	0	
df	7	
t Stat	-1.116	
P(T<=t) one-tail	0.151	
t Critical one-tail	1.895	
P(T<=t) two-tail	0.301	
t Critical two-tail	2.365	

We also evaluated whether the UGS with Indian Laurel trees where greener on average (Table 4). We find that there is a significant difference in the z-scores ($p<0.01$) for the UGS with mixed vegetation, versus the UGS with Indian Laurel trees. It appears that despite the fact that the UGS with Laurel trees did not reveal a significantly different rate of change, the UGS with Laurel trees are signifcantly greener overall than those with other vegetation types.

Table 4. t-test of Indian Laurel against mixed vegetation cover.

t-Test: Two-Sample Assuming Unequal Variances		
	mixed	***Indian Laurel***
Mean	-0.120	1.324
Variance	0.693	0.179
Observations	73	7
Hypothesized Mean Difference	0	
df	11	
t Stat	7.717	
P(T<=t) one-tail	4.593E-06	
t Critical one-tail	1.796	
P(T<=t) two-tail	9.185E-06	
t Critical two-tail	2.201	

2.5.4.2. The impact of the UGS size

To understand whether the size of the UGS impacts their greenness, we created a log-linear model linking the UGS size and the mean z-score over the 33-year period. The logistic regression model results (Figure 12) indicate that there is a significant relationship between the mean z-score and UGS size ($p < 0.01$). The majority of small UGS have a negative mean z-score and the z-score increases for larger UGS. A little more than 31% of the variability in greenness is explained by the size of UGS, with larger UGS being significantly greener. Other variables, such as the vegetation type, and level of maintenance are likely explaining aditional variability.

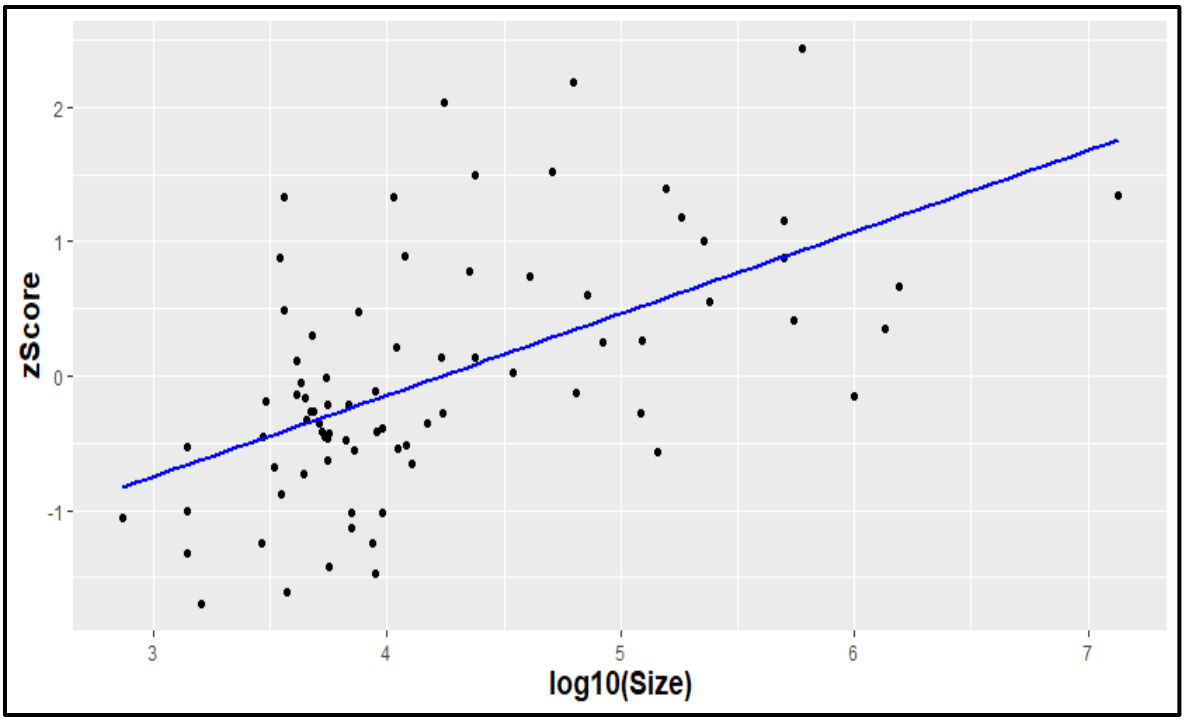

Figure 12. Log linear regression of UGS size and mean z-score of the 33-year period.

To understand if the size of UGS impacts how the greenness of the UGS changed over time, we created a log-linear model linking UGS size and the rate of change of the z-score over the 33-year period. The logistic regression model results (Figure 13) indicate no significant relationship between UGS size and UGS change ($p > 0.95$). Thus, while larger UGS are on average greener than smaller UGS, we do not find that larger UGS changed more or less over time than smaller UGS.

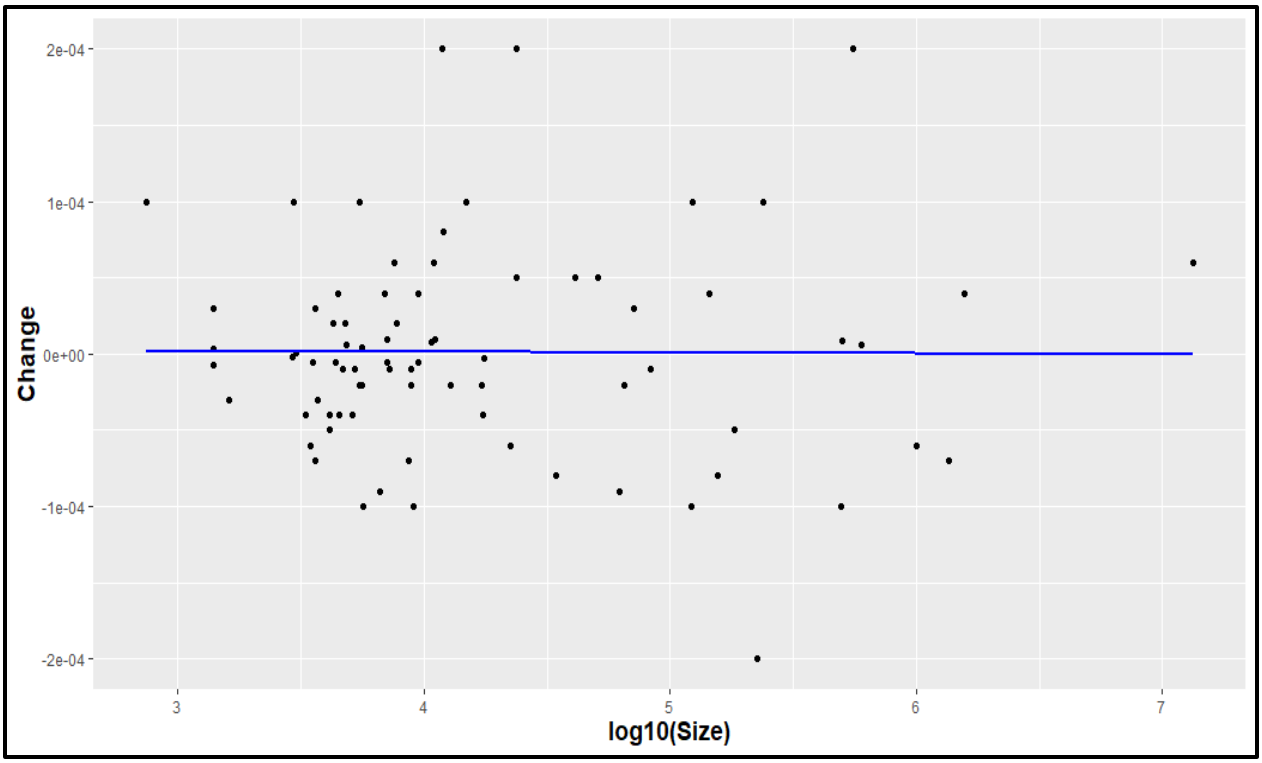

Figure 13. Log linear regression of UGS size and change of the 33-year period.

2.5.4.3. The impact of maintenance on UGS

In our last hypothesis, we test whether highly maintained and recently renovated UGS changed in greenness more significantly than less maintained UGS. We carried out a t-test to compare the change rate between 11 highly maintained or recently renovated UGS (according to our field observations) and all other (69 UGS). We did not find a significant difference ($p < 0.54$) between the two groups of parks. As a result, we reject our null hypothesis because the lack of evidence that the level of maintenance influences greenness in the UGSs over the 33-year period (Table 5). Figure 14 is an example of three selected parks that are highly maintained and their respective changes in NDVI, and their respective images from Google Earth.

Table 5. t-test of Laurel Indian against mixed vegetation cover.

t-Test: Two-Sample Assuming Unequal Variances		
	low maintenance	***high maintenance***
Mean	-6.928E-06	1.691E-05
Variance	3.145E-09	1.495E-08
Observations	69	11
Hypothesized Mean Difference	0	
df	11	
t Stat	-0.636	
P(T<=t) one-tail	0.269	
t Critical one-tail	1.796	
P(T<=t) two-tail	0.538	
t Critical two-tail	2.201	

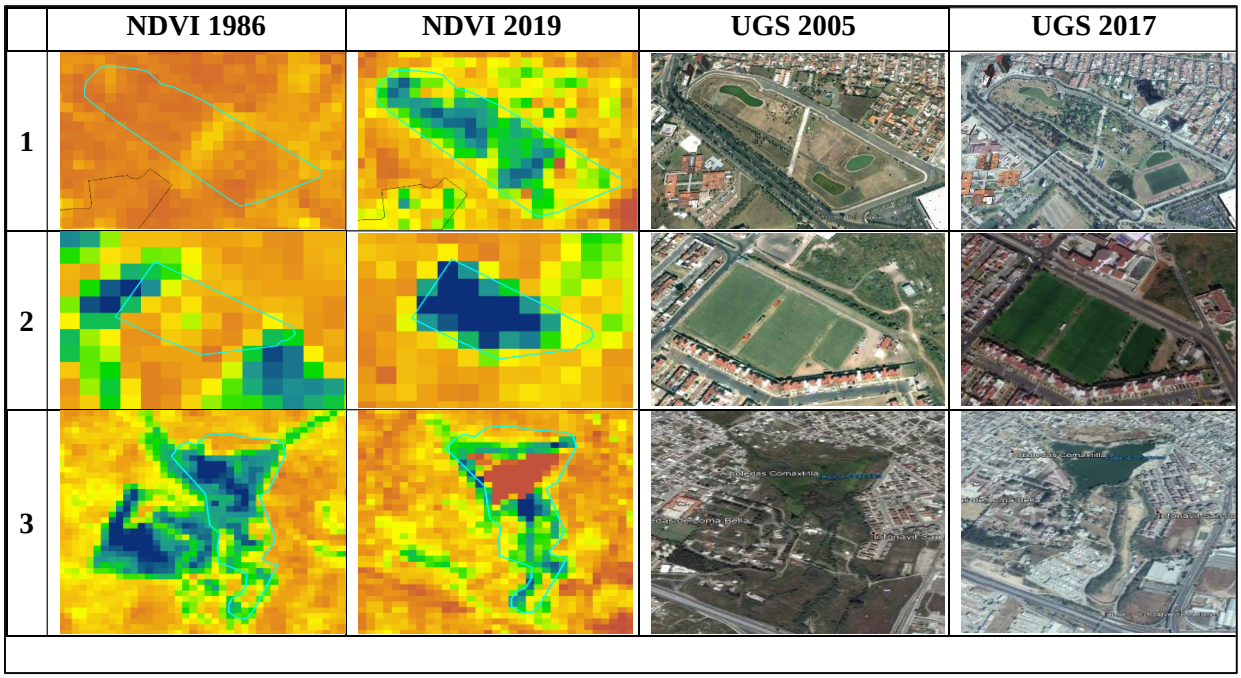

Figure 14. A visual comparison of NDVI in 1986 with 2019, and Google high-resolution images of 2005 and 2017. 1) is Jardin del Arte park, 2) is Soccer field, and 3) El Centenario/Chapulco Lake park.

2.5.5. Paseo of San Francisco and El Centenario/Chapulco Lake parks case study

While we did not find a statistically significant difference between the rate of change for highly maintained parks and the level of maintenance, we do want to highlight the development of some of the highly maintained parks specifically. We noticed from the eleven-highly mantained or recently renovated parks, that Paseo de San Francisco experienced the largest increase in greeness, while El Centenarion/Chapulco Lake decreased the most in greenness (Fig. 12).

a) **b)**

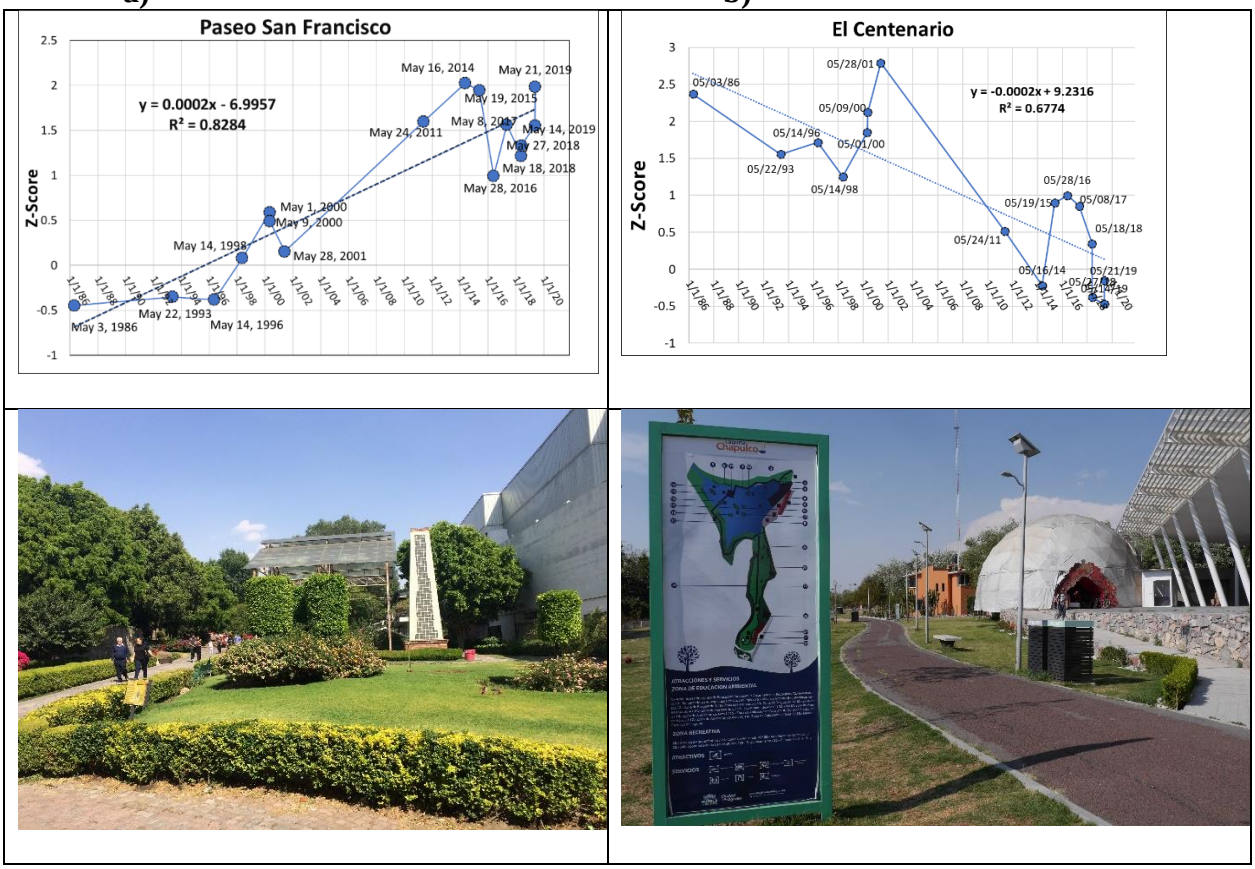

Figure 15. The graphs show the change in greenness of **a)** Paseo de San Francisco and **b)** El Centenario/Chapulco Lake during the 33-year period. The pictures reveal how these two diverging parks looked in 2018. Note that the Paseo de San Francisco is a very green city park with lush vegetation. El Centenario/Chapulco Lake on the other hand is dominated by impervious surfaces with limited shading and vegetation, and a large lake.

2.6 Results from LST

In the following section we present the results in the LST mean z-score and UGS size, LST change with UGS size, and the relationship of the LST mean z-score with the NDVI mean z-score formulated for May 1, 2000, May 24, 2011 and May 21, 2019 (see, Section 2.4.4).

2.6.1. LST change and UGS size

Figure 16 indicates a significant relationship ($p<0.01$) between the size of the UGS and the average Land Surface Temperature. Smaller (UGSs) were significantly warmer than larger UGS ($p<0.01$). Almost 50% of the variability in LST can be explained by the size of the UGS. Other biosphysical and human-induced variables such as location (nearer or further from the city

core), UGS greenness, vegetation cover type, and maintenance might explain the remaining variability in LST.

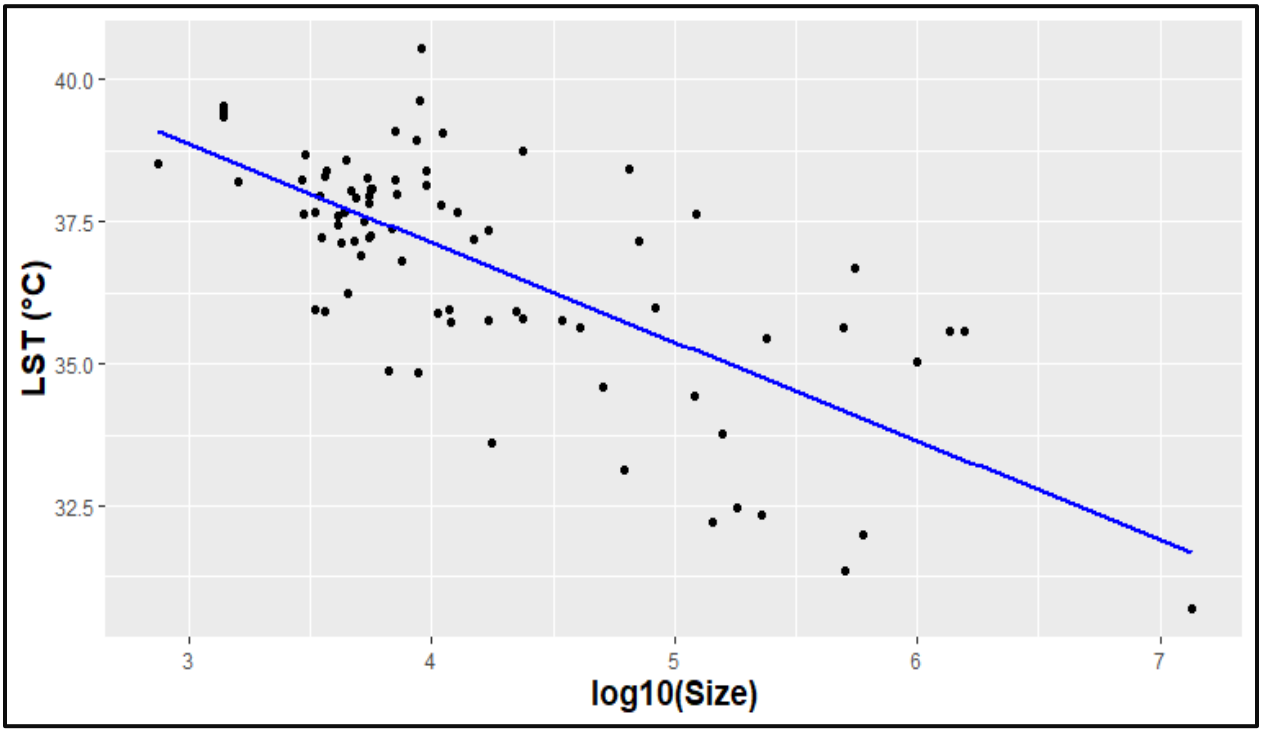

Figure 16. Log linear regression of size of 80 UGS and LST.

2.6.2 LST mean z-score and UGS size

We also evaluated how the rate of change of the LST over the period of 19 years (*using the data from 2000-19*) varied with the size of the UGS (Figure 17). We found a significant relationship ($p<0.01$) with larger UGS revealing cooling over time (negative slopes), while smaller UGS revealed slight warming or no change (rate of change was close to 0). Almost 30% of the change of the LST can be explained by the size of UGS. Other biosphysical and human-induced variables such as location (nearer or farther from the city core), USG greenness, vegetation cover, and maintenance might explain the remaining changes in LST.

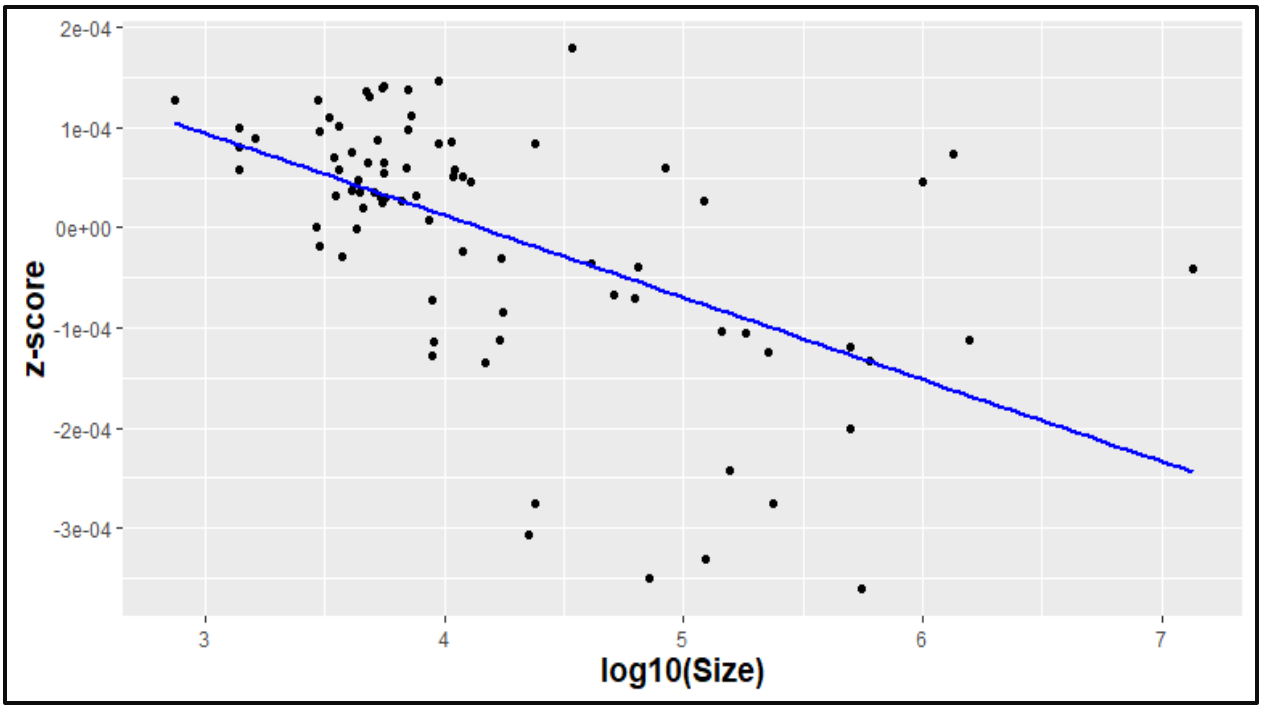

Figure 17. Log linear regression of LST mean z-score and change of Land Surface Temperature.

2.6.3. Detailed NDVI z-score and LST z-score analysis

To investigate the relationship between NDVI and LST we selected observations from three different years: 2000, 2011 and 2019 as examples. Figure 18 visualizes the data from May 1, 2000 and reveals a negative relationship between the NDVI and LST values ($p<0.01$), with an R-squared of 0.17. About 16.5% of the variability in the LST z-score of the UGS can be explained by the z-score of the NDVI. The relatively weak relationship shows that in general in the year 2000, greener parks were slightly cooler than browner parks and those differences depended on vegetation cover types. For example, parks covered with trees (C-B quadrant) were cooler than parks with grass cover (W-B quadrant) similarly size.

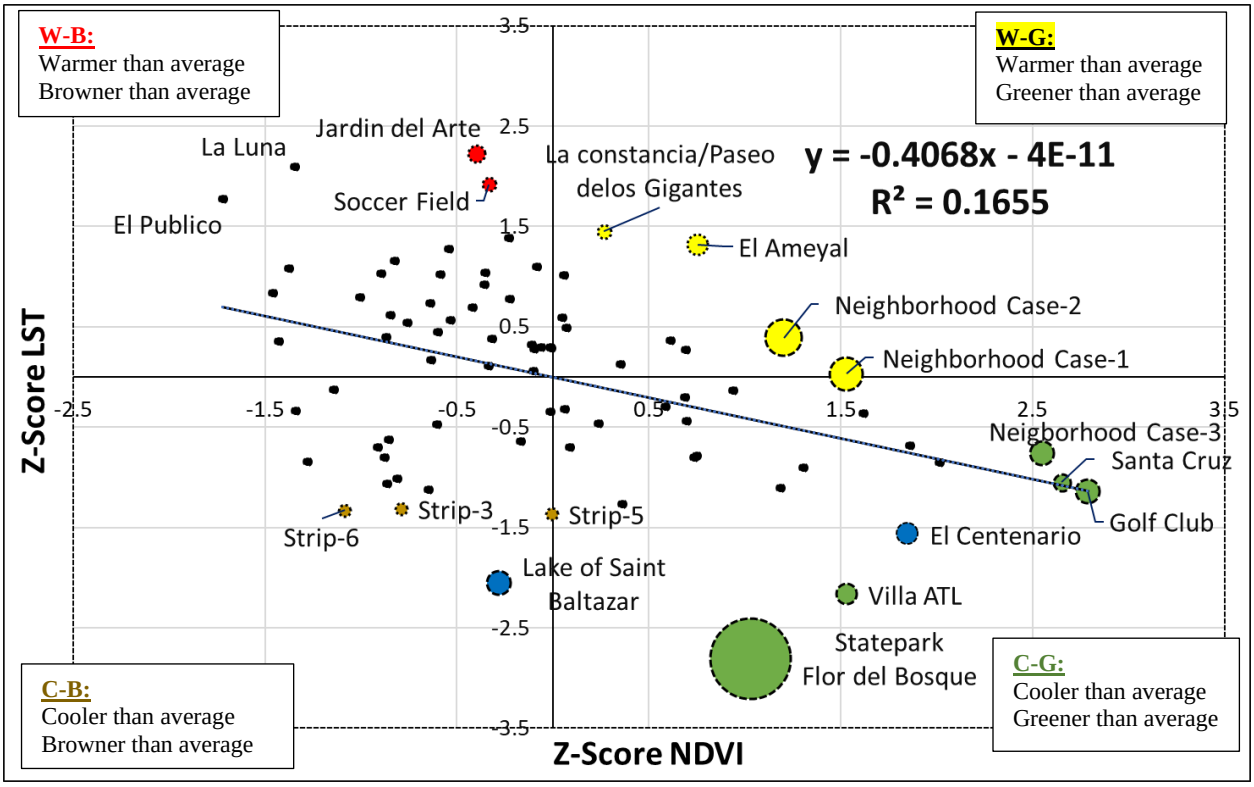

Figure 18. Relationship of NDVI z-score against the LST z-score for May 1, 2000 for each of the 80 urban green spaces. The colored circles represent the relative size of the UGS, and blue circles are UGS with waterbodies greater than 1 km^2.

UGS in the upper left quadrant (Warmer-Browner) and the lower right quadrant (Cooler-Greener), appear to follow the literature, which generally reports lower temperatures for areas with high green vegetation cover. UGSs in the lower left quadrant (Cooler-Browner) appear to behave against this idea, although at least one of those UGSs (Lake of San Baltazar) has a large waterbody, which could explain its relative coolness. UGSs in the upper right quadrant (Warmer-Greener), such as La Constancia/Paseo de Los Gigantes, El Ameyal, and Neighborhood Case-1 & Case-2, are relatively warm compared to their above average greenness.

The relationship between NDVI and LST appears to strengthen in time, with R^2_{adj} values increasing from 0.17 in 2000, to 0.37 in 2011 (Figure 19), and 0.42 in 2019 (Figure 20). This

strengthening might be a result of our UGS digitization being performed on modern high-resolution satellite imagery.

Most UGS in 2011 appear to match the general theory that greener areas are cooler. Exceptions are parks with large waterbodies (e.g. Lake of San Baltazar) where a browner than average UGS resulted in a cooler than average observation. This is not surprising considering that water is generally cooler than other land cover classes, and the NDVI values for water are generally low. Other UGS, such as the Soccer Field also divert from the regression line. The Soccer Field is relatively green; however, the green field provides no shading and as a result this UGS is slightly warmer than average.

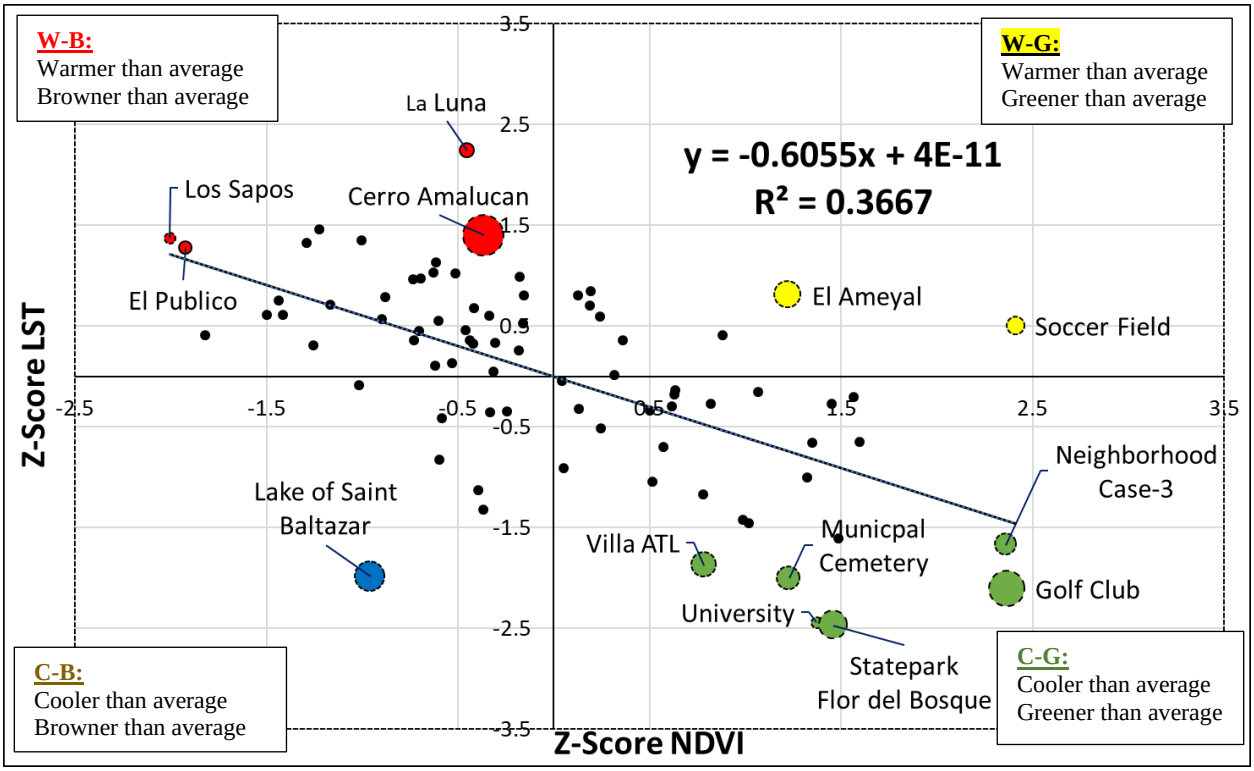

Figure 19. Relationship of NDVI z-score against the LST z-score for May 24, 2011 for each of the 80 urban green spaces. The colored circles represent the relative size of the UGS (except for University and Statepark Flor del Bosque, their sizes were reduced as they are close to each other) the one in blue has a significant waterbody, greater than 1km^2.

Figure 20 shows El Centenario/Chapulco Lake and Lake of Saint Baltazar (C-B quadrant) closer together both with extensive waterbodies on their surface. Not all UGS were fully established in 2000. El Centenario/Chapulco lake is a relatively new park that used to be an overgrown marshy area, after the establishment of this park it resulted in a reduction of the park area, and in vegetation cover but marshy water got cleaned resulted in lower LST compared to fig. 18. We found that highly maintained UGS generally increased in greenness (Paseo de San Francisco, Jardin del Arte, Ecopark Metropolitano de Puebla (includes a Baroque Museum) and Ecopark Mexican Revolution.

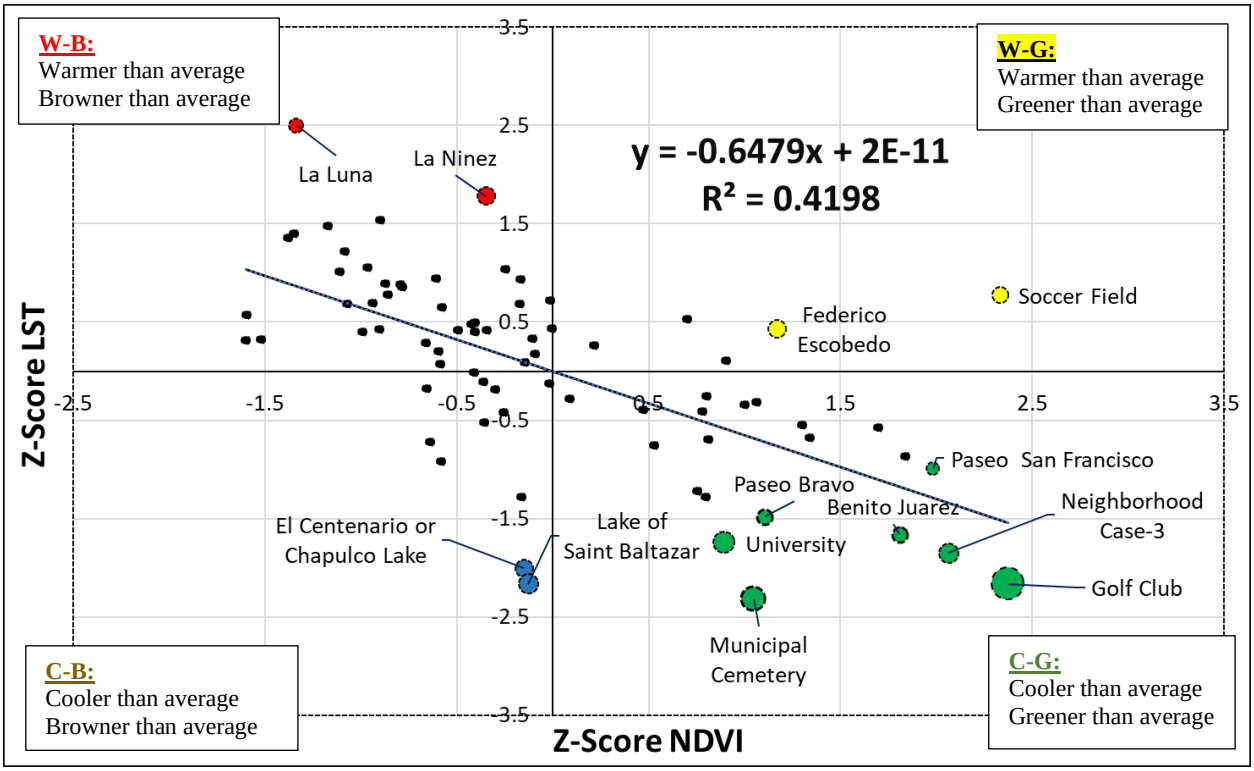

Figure 20. Relationship of NDVI z-score against the LST z-score for May 21, 2019 for each of the 80 urban green spaces. The colored circles represent the relative size of the UGS, and the ones in blue have waterbodies greater than 1 km^2.

The Soccer Field and El Ameyal also appear as outliers, with high NDVI values, and high land surface temperatures. These areas are covered with grass which does not produce shade, resulting in higher LST as well. While the opposite thing is observed with (C-G quadrant) parks (Paseo de San Francisco, Paseo Bravo, Benito Juarez and University) those parks mostly covered of Indian Laurel trees overt time they increased in height and in vegetation density, LST decreased over the 19-year. These results lead us to conclude that shade and canopy density are a vital variable for the remediation of UHI. Furthermore, an interesting relationship is observed for the Golf Club, which consistently has high NDVI and low LST. While the Golf Club is mostly covered with grass, it also has more than 40% of tree cover. This private Golf Club is also highly irrigated to keep the grass pristine, leading us to conclude that the soil has more moisture and potential evaporation from irrigation, causes lower LST.

2.7. Discussion

In this study, we have examined the NDVI and LST trajectories of 80 urban green spaces over a thirty-three-year period. We also analyzed the relationship of NDVI with LST after the year 2000. We visually inspected 73 of the 80 UGS, to understand land cover types and other characteristics of each of the UGS. Our study reveals that each UGS experienced change in NDVI differently, from biophysical processes, human induced changes and local climate impacts. We found significant variability in the results, with some UGS revealing significant greening while other UGS revealed greenness declines.

The result of this study is consistent with previous studies that reported contrasting NDVI changes by comparing specific neighborhoods in Chicago in 1998, with the same neighborhoods

in 2010 (Mackey et al. 2014). We also found contrasting NDVI changes and we also observed that standard deviation widened over time.

In this study, we were able to examine vegetation cover difference at a local scale, and we found that UGS with Indian Laurel were significantly greener than UGS with mixed vegetation cover, although we did not find that UGS with Indian Laurel changed at different rates. We also found that vegetation cover mattered for the LST relationship. UGS with grass such as the Soccer Field (in 2019), Neighborhood Case-1, and Neighborhood Case-2 (2010) had a relatively higher LST since these grassy UGS lacked shade. Other, studies also suggested that lower surface temperatures are due to shading, and high evapotranspiration (Alexander, 2020), vegetation types, and canopy density (Feyisa et al. 2014), and tree cover (Dugord et al. 2014). Soil temperature differences beneath trees and shrubs are lower compared to herbaceous and grass cover in the summer months (Edmonson et al., 2016). Similarly, surface temperature of grass is lower than asphalt or concrete (Ziter et al. 2019)

Similar, to what other studies have found, we found that UGS with large water bodies (>128,889 m^2) are generally cooler (Chen et al. 2012; & Kong et al. 2014). El Centenario/Chapulco Lake (227,050 m^2) and Lake of Saint Baltazar (143,629 m^2) had lower LST compared to similar size UGS without waterbodies. Water bodies and dense urban green infrastructure were found to dampen LST in two Indian cities (Ramaiah et al. 2020). Water has a higher heat capacity than vegetation and most of the solar visible solar radiation is absorbed (Gunawardena et al. 2017; & Cheng et al. 2006), and subsequently released later. As a result, while water might be cooler in daytime images, it would be warmer during the night.

We demonstrated that large UGS are generally greener compared to smaller UGS, which is consistent with what other studies have concluded. By examining thirty-nine parks, Cheng et

al. (2015) concluded that larger parks provide higher NDVI values, resulting also in maximum cooling effect (Lin et al. 2015). Other studies also conclude that vegetation, water, and impervious surface cover determine LST (Cheng et al., 2006, Ezimand et al. 2018; Owen et al., 1998, Weng et al. 2004).

Multiple studies have been conducted investigating the relation between urbanization and UHI. One study found a positive relationship between the urban area and LST during the daytime for 500 urban areas in the USA (Li et al. 2017). They also found that the size of the urban area can explain up to 87% of the variance in UHI. As urbanization continues to increase worldwide it is important to preserve and build more urban green infrastructure to reduce surface and air temperatures. Urban green infrastructure can reduce the energy demand and consumption for cooling (Akbari et al., 1997) and alleviate UHI impact (Chen et al. 2020).

Previous studies that have examined UGSs relationships with UHI on a city scale have predominantly used just one year, a summer season, or in some cases one date of data (Bokaie et al. 2016; Chang and Li, 2014; Cheng et al. 2014; Cao et al. 2010), with the exception of Mackey et al. (2012) examined UGS in Chicago for a twelve-year period (1998-2010). Similarly, many studies treat UGSs as static (Rotem-Mindali et al. 2015; Saaroni et al. 2018; Schwarz et al. 2012; Zhou et al. 2011). Cognizant to this limitation, our work used thirty years of data and treated the UGS as transient entities, assuming changes can be from natural processes such as senescence, induced changes from human activities. Using z-scores to investigate changes within UGS and across UGS, allowed us to understand variability in greenness.

Field observation allowed us to learn about each park and helped to interpret our results better. For example, park Federico Escobedo was mostly covered by Jacaranda trees (Fig. 6) and was found ‘greener’ and warmer than average in May 21, 2019 (Fig. 19). The month of May is

the flowering season of the Jacaranda flowers resulting in higher NDVI, but also higher in LST as the flowers are mainly in the upper layer of the canopy resulting in limited shade, and warmer than average temperatures. Canopy layers in vegetation result in strong shading and with robust shade results in lower LST. Using field observations for 73 of the 80 UGSs, allowed us to learn differences in land cover, vegetation types, vegetation changes (as is the case with Jacaranda flowering), maintenance and infrastructure characteristics for each UGS, and social aspects. For example, in some parks there were street food vendors (e.g. Paseo Bravo park); El Tamborcito park (little drum) had an installation honoring murdered women and immigrant issues, to advocate for equal rights; one park had a training facility for acrobatics and tumbling (El Centenario park). Some parks have fancy services and infrastructure, while others lack services and basic amenities.

Field observation enhanced our understanding and interpretation of the results. While we visited the park, we often talked to park users to learn about the story of the park. For example, Park El Centenario/Chapulco Lake is a relatively new park in which its vegetation cover was reduced as impervious surfaces were added. However, during renovation, the water body was also cleaned up, several aeration systems were installed to keep to water circulated, and the LST values, which are typically lower for water bodies, dropped significantly. While, renovations in other parks, such as in Los Fuertes and El Centenario/Chapulco Lake, have resulted in a vegetation reduction. In other renovated UGS such as Los Fuertes (monuments and statues of the battle of Cinco de Mayo, museum, coffee shops), and La Constancia/Paseo de los Gigantes, which is a model park showcasing iconic buildings from around world, a museum, and a coffee shop, aesthetic and cultural displays are prioritized over environmental benefits.

Also, visiting 73-UGSs created a sense of place and connection to each park. For example, the names of the UGSs range from priest, politician, beauty pageant, animal names such as Los Sapos (frogs) and Las Hadas (fairies), and organizations names such as the Rotario Internacional park (International Rotary). Similarly, from field observations, we learned vegetation cover differences. For example, we learned that Eucalyptus trees dominate the Cerro Amalucan park (Fig. 6). Eucalyptus have a single main stem, and they are fast-growing trees, ranging from 10 to 60 m. However, with low canopy density and with long and slender leaves (7- 10 cm) pointing downward, these trees generate limited shade. Cerro Amalucan park is one of the biggest UGS in our study (see visualization summary Fig. 9), which is the large yellow polygon in East of the city. The second yellow is the Los Fuertes parks which also has Eucalyptus trees and other vegetation and is about 45% covered with impervious surfaces that include roads, parking lots, museums, and a statue with personages commemorating the Cinco de Mayo, Battle of Puebla.

Lastly, our work intends to bridge the gap of what Zhou et al. (2019) have called geographic asymmetries in the cities studied for UHI. Most UHI and studies of urban green spaces predominantly look at parks that are concentrated in just a handful of countries and their respective cities. While some UHI studies have been conducted in Puebla (Mexico), to our knowledge, this is the first study where optical and thermal remotely sensed data are used to examine UGS and LST.

2.8. Conclusion

This study intends to reduce the gaps in scholarship on asymmetries that Zhou and others identified in their literature review of UHI (Zhou et al. 2018). They identified that

limited UHI and urban green space studies have been conducted in other cities locates in other countries except cities in China, Unites States of America, Europe. It examined the dynamic nature of the 80 UGS for a thirty-three-year period. Lastly, it included field observations to examine the characteristics and vegetation cover types from the UGS. We found that small UGS are not as effective at reducing UHI as larger UGS. Similarly, the cooling intensity directly depends on land cover characteristics, as large UGS with portions of impervious surfaces or bare land might not be as effective in temperature reduction as UGS with vegetated areas. Similar size UGS with similar NDVI results, presented different LST values, and this difference was largely dependent on shadow effects, for example UGS mostly covered with trees had lower LST than UGS primarily covered with grasses. UGS with large water bodies were more effective at reducing daytime LST, although we did not investigate nighttime data.

As urban populations continue to increase, urbanization encroachment in the vegetated landscapes is more likely to continue, resulting in the increase of UHI. For cities located in the lower latitudes, the UHI is more acute than for cities in higher latitudes (Campbell et al. 2018) because cities in the lower latitudes receive more solar radiation year around and in the summer months insolation is further exacerbated. Monitoring the health of UGSs and their relationship with LST is important to better understand how cities can implement and maintain urban green infrastructure.

The inclusion of field observation allowed us to further understand vegetation cover types for each UGS. UGSs vegetated with Indian Laurel trees were greener than UGS with mixed cover. Similarly, UGSs covered with Indian Laurel trees were stable compared to UGSs with mixed vegetation cover. This stability in greenness might be because Indian Laurel does not shed all its leaves in one season but instead sheds them year around. Also, Indian Laurel trees have dense

canopy layers with oblate shape which provide more shade resulting in more cooling than, for example Eucalyptus trees, with stringy/elongated leaves pointing down. While newly planted Indian Laurel trees require intense watering to stablish their roots, once the trees are established watering can be eliminated as they area drought resistant compared to grass, flowers, and other ornamental shrubs. Planting Indian Laurel trees in UGSs in Puebla can be a good xeriscaping practices and yields the most ecosystem services compared to other succulent plants, grass or other ornamental shrubs. Although, Indian Laurel trees are not native to Puebla, they do fit the 'right plant and the right place' concept (Beck, 2013), because they grow well in Puebla's climate.

Chapter 3. Conclusion

Cities provide opportunities, and they also face social and environmental challenges. This study addressed the importance of UGSs to reduce UHI impacts. UHI is one of the many environmental challenges' cities face, as discussed in the previous chapter ample research conclude that UGSs reduce UHI impact, and associated energy demands for air conditioning while providing other ecosystem services (Walter, 2018; Saaratoni et al. 2018). UGSs contribute to the well-being of the residents as discussed in previous chapters. Conscious of UGSs multi-layer benefits, some cities in Latin America (Mexico City; Bogota, Colombia; Buenos Aires, Argentina; Santiago, Chile, etc.) are actively implementing UGSs and some are in the early stages of becoming a 'smart city' (Calderon et al. 2017). Similarly, other cities embrace and actively promote urban green infrastructure. For example, in the City of Portland (Oregon) the Portland Forest park, encompasses 5,200 acres and is considered one of the largest urban forest parks in the United States (https://www.portland.gov/parks/forest-park). No cities are more committed to preserving and maintaining urban green areas than the City of Singapore, which currently has more than 50% of tree and vegetation cover (Henderson, Joan C. 2012), and the City of Vancouver which is moving beyond implementing UGSs and is actively working toward urban sustainability (Affolderbach & Schulz, 2017).

It is important to mention that many of the initiatives and actions to preserving, and building green infrastructure are led mainly by municipal governments. Although in Puebla's case, the establishment and renovation of parks required partnership between the state governor Rafael Moreno Valle Rosas (2011-2017) and three different mayors (Eduardo Rivera Perez (2011-2014), Jose Antonio Gali Fayad (2014-2017), and Luis Banck Serrato (2016-2018). In this study, we conclude that not every UGS contributes the same cooling intensity. We found

that large parks contribute more to reducing and mitigating the UHI effect especially if a park had dense tree and dense canopy layers, and a series of small parks might not be as effective in temperature regulation. The land cover types are also important; for example, UGS with water bodies over 1 km^2 provided the most cooling intensity compared to other UGS with smaller water bodies. Some of the larger parks were very well maintained, but had too much impervious surfaces, and consequently were not contributing to reducing LST.

This work has shortcomings, the inclusion of landscape metrics (patch, edge, and shape density) could have furthered our understandings of the park characteristics and their influence on LST. Similarly, including other data such as from the ECOsystem Spaceborne Thermal Radiometer Experiment in Space Station (ECOSTRESS) which measures both evaporation and transpiration of the vegetation would have allowed us a better understanding of temperature changes over diurnal periods. ECOSTRESS, like Landsat, senses thermal infrared brightness (https://ecostress.jpl.nasa.gov/data). ECOSTRESS is mounted to the International Space Station, and as a result the sensor has no fixed overpass time, allowing for images taken at different times for the day and night (Cha et al, 2017). Nighttime data are especially relevant, as the UHI effect is more acute during the night, when impervious surfaces release most radiant energy. Also, if LiDAR data were available in the study area, we could have developed a map of tree crowns and develop a shadow model. Our investigation revealed the effect of Indian Laurel trees, which generally provide important shading. In the future incorporating ECOSTRESS data, landscape metrics, and LiDAR data could result in a deeper understanding of the biophysical changes in the vegetation, canopy, shadow effects and their relationship with LST for each of the green infrastructures.

References

Abarca, K. M. N., De Lara, C. F., Hernandez, A. S., & Leon, M. T. (2018). Evaluation of urban heat island for Puebla City, Mexico. *Sustainable Development and Planning*, 867–879. https://doi.org/10.2495/SDP180731

Affolderbach, J., & Schulz, C. (2017). Positioning Vancouver through urban sustainability strategies? The Greenest City 2020 Action Plan. *Journal of Cleaner Production*, *164*, 676–685. https://doi.org/10.1016/j.jclepro.2017.06.234

Alexander, C. (2020). Normalised difference spectral indices and urban land cover as indicators of land surface temperature (LST). *International Journal of Applied Earth Observation and Geoinformation*, *86*, 102013. https://doi.org/10.1016/j.jag.2019.102013

Anuja, A. R. (2018). Analysis of Factors Triggering Distress Migration in Bundelkhand Region of Central In. *Economic Affairs*, *63*(4). https://doi.org/10.30954/0424-2513.4.2018.31

Ballinas, M., & Barradas, V. L. (2016). The Urban Tree as a Tool to Mitigate the Urban Heat Island in Mexico City: A Simple Phenomenological Model. *Journal of Environmental Quality*, *45*(1), 157–166. https://doi.org/10.2134/jeq2015.01.0056

Beck, T. (2013). Right Plant, Right Place: Biogeography and Plant Selection. In T. Beck, *Principles of Ecological Landscape Design* (pp. 7–31). Island Press/Center for Resource Economics. https://doi.org/10.5822/978-1-61091-199-3_1

Bokaie, M., Zarkesh, M. K., Arasteh, P. D., & Hosseini, A. (2016). Assessment of Urban Heat Island based on the relationship between land surface temperature and Land Use/ Land Cover in Tehran. *Sustainable Cities and Society*, *23*, 94–104. https://doi.org/10.1016/j.scs.2016.03.009

Campbell, S., Remenyi, T. A., White, C. J., & Johnston, F. H. (2018). Heatwave and health impact research: A global review. *Health & Place*, *53*, 210–218. https://doi.org/10.1016/j.healthplace.2018.08.017

Cha, J. S., Rodriguez, J. I., & Carroll, B. (n.d.). *Thermal Control System of the ECOsystem Spaceborne Thermal Radiometer Experiment on Space Station*. 9.

Chang, C.-R., & Li, M.-H. (2014). Effects of urban parks on the local urban thermal environment. *Urban Forestry & Urban Greening*, *13*(4), 672–681. https://doi.org/10.1016/j.ufug.2014.08.001

Chen, J., Jin, S., & Du, P. (2020). Roles of horizontal and vertical tree canopy structure in mitigating daytime and nighttime urban heat island effects. *International Journal of Applied Earth Observation and Geoinformation*, *89*, 102060. https://doi.org/10.1016/j.jag.2020.102060

Chen, X.-L., Zhao, H.-M., Li, P.-X., & Yin, Z.-Y. (2006). Remote sensing image-based analysis of the relationship between urban heat island and land use/cover changes. *Remote Sensing of Environment*, *104*(2), 133–146. https://doi.org/10.1016/j.rse.2005.11.016

Cheng, X., Wei, B., Chen, G., Li, J., & Song, C. (2015). Influence of Park Size and Its Surrounding Urban Landscape Patterns on the Park Cooling Effect. *Journal of Urban Planning and Development*, *141*(3), A4014002. https://doi.org/10.1061/(ASCE)UP.1943-5444.0000256

Cui, Y. Y., & de Foy, B. (2012). Seasonal Variations of the Urban Heat Island at the Surface and the Near-Surface and Reductions due to Urban Vegetation in Mexico City. *Journal of Applied Meteorology and Climatology*, *51*(5), 855–868. https://doi.org/10.1175/JAMC-D-11-0104.1

Duan, J., Wang, Y., Fan, C., Xia, B., & de Groot, R. (2018). Perception of Urban Environmental Risks and the Effects of Urban Green Infrastructures (UGIs) on Human Well-being in Four Public Green Spaces of Guangzhou, China. *Environmental Management*, *62*(3), 500–517. https://doi.org/10.1007/s00267-018-1068-8

Dugord, P.-A., Lauf, S., Schuster, C., & Kleinschmit, B. (2014). Land use patterns, temperature distribution, and potential heat stress risk – The case study Berlin, Germany. *Computers, Environment and Urban Systems*, *48*, 86–98. https://doi.org/10.1016/j.compenvurbsys.2014.07.005

Eakin, H., & Lemos, M. C. (2006). Adaptation and the state: Latin America and the challenge of capacity-building under globalization. *Global Environmental Change*, *16*(1), 7–18. https://doi.org/10.1016/j.gloenvcha.2005.10.004

Feyisa, G. L., Dons, K., & Meilby, H. (2014). Efficiency of parks in mitigating urban heat island effect: An example from Addis Ababa. *Landscape and Urban Planning*, *123*, 87–95. https://doi.org/10.1016/j.landurbplan.2013.12.008

Fu, W. Q. (2006). Radiative Transfer. In *Atmospheric Science* (pp. 113–152). Elsevier. https://doi.org/10.1016/B978-0-12-732951-2.50009-0

Gibson, S. C. (2018). "Let's go to the park." An investigation of older adults in Australia and their motivations for park visitation. *Landscape and Urban Planning*, *180*, 234–246. https://doi.org/10.1016/j.landurbplan.2018.08.019

Glenn, E., Huete, A., Nagler, P., & Nelson, S. (2008). Relationship Between Remotely-sensed Vegetation Indices, Canopy Attributes and Plant Physiological Processes: What Vegetation Indices Can and Cannot Tell Us About the Landscape. *Sensors*, *8*(4), 2136–2160. https://doi.org/10.3390/s8042136

Gunawardena, K. R., Wells, M. J., & Kershaw, T. (2017). Utilising green and bluespace to mitigate urban heat island intensity. *Science of The Total Environment*, *584–585*, 1040–1055. https://doi.org/10.1016/j.scitotenv.2017.01.158

Hamada, S., & Ohta, T. (2010). Seasonal variations in the cooling effect of urban green areas on surrounding urban areas. *Urban Forestry & Urban Greening*, *9*(1), 15–24. https://doi.org/10.1016/j.ufug.2009.10.002

Hamilton, S. K., Hussain, M. Z., Lowrie, C., Basso, B., & Robertson, G. P. (2016). *Evapotranspiration is resilient in the face of land cover and climate change in a humid temperate catchment* [Preprint]. Ecology. https://doi.org/10.1101/075598

Han, H. (2017). Singapore, a Garden City: Authoritarian Environmentalism in a Developmental State. *The Journal of Environment & Development*, *26*(1), 3–24. https://doi.org/10.1177/1070496516677365

Huete, A. R., Jackson, R. D., & Post, D. F. (1985). Spectral response of a plant canopy with different soil backgrounds. *Remote Sensing of Environment*, *17*(1), 37–53. https://doi.org/10.1016/0034-4257(85)90111-7

Hulley, G. C., & Hook, S. J. (2009). The North American ASTER Land Surface Emissivity Database (NAALSED) Version 2.0. *Remote Sensing of Environment*, *113*(9), 1967–1975. https://doi.org/10.1016/j.rse.2009.05.005

Hulley, G. C., Hook, S. J., Abbott, E., Malakar, N., Islam, T., & Abrams, M. (2015). The ASTER Global Emissivity Dataset (ASTER GED): Mapping Earth's emissivity at 100-meter spatial scale. *Geophysical Research Letters*, *42*(19), 7966–7976. https://doi.org/10.1002/2015GL065564

Hulley, G., Hook, S., Fisher, J., & Lee, C. (2017). ECOSTRESS, A NASA Earth-Ventures Instrument for studying links between the water cycle and plant health over the diurnal cycle. *2017 IEEE International Geoscience and Remote Sensing Symposium (IGARSS)*, 5494–5496. https://doi.org/10.1109/IGARSS.2017.8128248

Jauregui, E., Godinez, L., & Cruz, F. (1992). Aspects of heat-island development in Guadalajara, Mexico. *Atmospheric Environment. Part B. Urban Atmosphere*, *26*(3), 391–396. https://doi.org/10.1016/0957-1272(92)90014-J

Jauregui, Ernesto. (1993). Mexico City's urban heat island revisited. *ERDKUNDE*, *47*(3). https://doi.org/10.3112/erdkunde.1993.03.03

Kondo, M., Fluehr, J., McKeon, T., & Branas, C. (2018). Urban Green Space and Its Impact on Human Health. *International Journal of Environmental Research and Public Health*, *15*(3), 445. https://doi.org/10.3390/ijerph15030445

Kong, F., Yin, H., Wang, C., Cavan, G., & James, P. (2014). A satellite image-based analysis of factors contributing to the green-space cool island intensity on a city scale. *Urban Forestry & Urban Greening*, *13*(4), 846–853. https://doi.org/10.1016/j.ufug.2014.09.009

Kothencz, G., Kolcsár, R., Cabrera-Barona, P., & Szilassi, P. (2017). Urban Green Space Perception and Its Contribution to Well-Being. *International Journal of Environmental Research and Public Health*, *14*(7), 766. https://doi.org/10.3390/ijerph14070766

Leal Filho, W., Echevarria Icaza, L., Neht, A., Klavins, M., & Morgan, E. A. (2018). Coping with the impacts of urban heat islands. A literature based study on understanding urban heat vulnerability and the need for resilience in cities in a global climate change context. *Journal of Cleaner Production*, *171*, 1140–1149. https://doi.org/10.1016/j.jclepro.2017.10.086

Li, H., Zhou, Y., Li, X., Meng, L., Wang, X., Wu, S., & Sodoudi, S. (2018a). A new method to quantify surface urban heat island intensity. *Science of The Total Environment*, *624*, 262–272. https://doi.org/10.1016/j.scitotenv.2017.11.360

Li, H., Zhou, Y., Li, X., Meng, L., Wang, X., Wu, S., & Sodoudi, S. (2018b). A new method to quantify surface urban heat island intensity. *Science of The Total Environment*, *624*, 262–272. https://doi.org/10.1016/j.scitotenv.2017.11.360

Lin, W., Yu, T., Chang, X., Wu, W., & Zhang, Y. (2015). Calculating cooling extents of green parks using remote sensing: Method and test. *Landscape and Urban Planning*, *134*, 66–75. https://doi.org/10.1016/j.landurbplan.2014.10.012

Liu, Y., Peng, J., & Wang, Y. (2018). Efficiency of landscape metrics characterizing urban land surface temperature. *Landscape and Urban Planning*, *180*, 36–53. https://doi.org/10.1016/j.landurbplan.2018.08.006

Mackey, C. W., Lee, X., & Smith, R. B. (2012). Remotely sensing the cooling effects of city scale efforts to reduce urban heat island. *Building and Environment*, *49*, 348–358. https://doi.org/10.1016/j.buildenv.2011.08.004

Maimaitiyiming, M., Ghulam, A., Tiyip, T., Pla, F., Latorre-Carmona, P., Halik, Ü., Sawut, M., & Caetano, M. (2014). Effects of green space spatial pattern on land surface temperature: Implications for sustainable urban planning and climate change adaptation. *ISPRS Journal of Photogrammetry and Remote Sensing*, *89*, 59–66. https://doi.org/10.1016/j.isprsjprs.2013.12.010

McKinney, M. L. (2002). Urbanization, Biodiversity, and Conservation. *BioScience*, *52*(10), 883. https://doi.org/10.1641/0006-3568052

Polydoros, A., & Cartalis, C. (2015). Use of Earth Observation based indices for the monitoring of built-up area features and dynamics in support of urban energy studies. *Energy and Buildings*, *98*, 92–99. https://doi.org/10.1016/j.enbuild.2014.09.060

Qin, Z., Karnieli, A., & Berliner, P. (2001). A mono-window algorithm for retrieving land surface temperature from Landsat TM data and its application to the Israel-Egypt border region. *International Journal of Remote Sensing*, *22*(18), 3719–3746. https://doi.org/10.1080/01431160010006971

Ramaiah, M., Avtar, R., & Rahman, Md. M. (2020). Land Cover Influences on LST in Two Proposed Smart Cities of India: Comparative Analysis Using Spectral Indices. *Land*, *9*(9), 292. https://doi.org/10.3390/land9090292

Ren, Z., He, X., Zheng, H., Zhang, D., Yu, X., Shen, G., & Guo, R. (2013). Estimation of the Relationship between Urban Park Characteristics and Park Cool Island Intensity by Remote Sensing Data and Field Measurement. *Forests*, *4*(4), 868–886. https://doi.org/10.3390/f4040868

Renard, F., Alonso, L., Fitts, Y., Hadjiosif, A., & Comby, J. (2019). Evaluation of the Effect of Urban Redevelopment on Surface Urban Heat Islands. *Remote Sensing*, *11*(3), 299. https://doi.org/10.3390/rs11030299

Rivera, E., Antonio-Némiga, X., Origel-Gutiérrez, G., Sarricolea, P., & Adame-Martínez, S. (2017). Spatiotemporal analysis of the atmospheric and surface urban heat islands of the Metropolitan Area of Toluca, Mexico. *Environmental Earth Sciences*, *76*(5), 225. https://doi.org/10.1007/s12665-017-6538-4

Rotem-Mindali, O. (2015). The role of local land-use on the urban heat island effect of Tel Aviv as assessed from satellite remote sensing. *Applied Geography*, 9.

Saaroni, H., Amorim, J. H., Hiemstra, J. A., & Pearlmutter, D. (2018). Urban Green Infrastructure as a tool for urban heat mitigation: Survey of research methodologies and findings across different climatic regions. *Urban Climate*, *24*, 94–110. https://doi.org/10.1016/j.uclim.2018.02.001

Santamouris, M., Cartalis, C., Synnefa, A., & Kolokotsa, D. (2015). On the impact of urban heat island and global warming on the power demand and electricity consumption of buildings—A review. *Energy and Buildings*, *98*, 119–124. https://doi.org/10.1016/j.enbuild.2014.09.052

Schwarz, N., Schlink, U., Franck, U., & Großmann, K. (2012). Relationship of land surface and air temperatures and its implications for quantifying urban heat island indicators—An application for the city of Leipzig (Germany). *Ecological Indicators*, *18*, 693–704. https://doi.org/10.1016/j.ecolind.2012.01.001

Sekertekin, A., & Bonafoni, S. (2020). Land Surface Temperature Retrieval from Landsat 5, 7, and 8 over Rural Areas: Assessment of Different Retrieval Algorithms and Emissivity Models and Toolbox Implementation. *Remote Sensing*, *12*(2), 294. https://doi.org/10.3390/rs12020294

Tang, H., & Li, Z.-L. (2014). *Quantitative Remote Sensing in Thermal Infrared*. Springer Berlin Heidelberg. https://doi.org/10.1007/978-3-642-42027-6

Trlica, A., Hutyra, L. R., Schaaf, C. L., Erb, A., & Wang, J. A. (2017). Albedo, Land Cover, and Daytime Surface Temperature Variation Across an Urbanized Landscape: ALBEDO OF URBAN LANDSCAPE. *Earth's Future*, *5*(11), 1084–1101. https://doi.org/10.1002/2017EF000569

Tucker, C. J. (n.d.). *Red and Photographic Infrared l,lnear Combinations for Monitoring Vegetation*. 24.

Vidrih, B., & Medved, S. (2013). Multiparametric model of urban park cooling island. *Urban Forestry & Urban Greening*, *12*(2), 220–229. https://doi.org/10.1016/j.ufug.2013.01.002

Villanueva-Solis, J. (2017). Urban Heat Island Mitigation and Urban Planning: The Case of the Mexicali, B. C. Mexico. *American Journal of Climate Change*, *06*(01), 22–39. https://doi.org/10.4236/ajcc.2017.61002

von Döhren, P., & Haase, D. (2015). Ecosystem disservices research: A review of the state of the art with a focus on cities. *Ecological Indicators*, *52*, 490–497. https://doi.org/10.1016/j.ecolind.2014.12.027

Voogt, J. A., & Oke, T. R. (2003). Thermal remote sensing of urban climates. *Remote Sensing of Environment*, *86*(3), 370–384. https://doi.org/10.1016/S0034-4257(03)00079-8

Windahl, E., & de Beurs, K. M. (2016). An intercomparison of Landsat land surface temperature retrieval methods under variable atmospheric conditions using in situ skin temperature. *International Journal of Applied Earth Observation and Geoinformation*, *51*, 11–27. https://doi.org/10.1016/j.jag.2016.04.003

Yagüe, C., Zurita, E., & Martinez, A. (1991). Statistical analysis of the Madrid urban heat island. *Atmospheric Environment. Part B. Urban Atmosphere*, *25*(3), 327–332. https://doi.org/10.1016/0957-1272(91)90004-X

Yuan, F., & Bauer, M. E. (2007). Comparison of impervious surface area and normalized difference vegetation index as indicators of surface urban heat island effects in Landsat imagery. *Remote Sensing of Environment*, *106*(3), 375–386. https://doi.org/10.1016/j.rse.2006.09.003

Zhang, S., & Zhou, W. (2018). Recreational visits to urban parks and factors affecting park visits: Evidence from geotagged social media data. *Landscape and Urban Planning, 180,* 27–35. https://doi.org/10.1016/j.landurbplan.2018.08.004

Zhang, Y., Murray, A. T., & Turner, B. L. (2017). Optimizing green space locations to reduce daytime and nighttime urban heat island effects in Phoenix, Arizona. *Landscape and Urban Planning*, *165*, 162–171. https://doi.org/10.1016/j.landurbplan.2017.04.009

Zhao, C., Jensen, J., Weng, Q., & Weaver, R. (2018). A Geographically Weighted Regression Analysis of the Underlying Factors Related to the Surface Urban Heat Island Phenomenon. *Remote Sensing*, *10*(9), 1428. https://doi.org/10.3390/rs10091428

Zhou, D., Xiao, J., Bonafoni, S., Berger, C., Deilami, K., Zhou, Y., Frolking, S., Yao, R., Qiao, Z., & Sobrino, J. (2018). Satellite Remote Sensing of Surface Urban Heat Islands: Progress, Challenges, and Perspectives. *Remote Sensing*, *11*(1), 48. https://doi.org/10.3390/rs11010048

Zhou, W., Huang, G., & Cadenasso, M. L. (2011). Does spatial configuration matter? Understanding the effects of land cover pattern on land surface temperature in urban landscapes. *Landscape and Urban Planning*, *102*(1), 54–63. https://doi.org/10.1016/j.landurbplan.2011.03.009